

Local EGOP for Continuous Index Learning

Alex Kokot

University of Washington,
Department of Statistics

Anand Hemmady

University of Washington,
Department of Biostatistics

Vydhourie Thiyyageswaran

University of Washington,
Department of Statistics

Marina Meila

University of Waterloo,
School of Computer Science

Abstract

We introduce the setting of continuous index learning, in which a function of many variables varies only along a small number of directions at each point. For efficient estimation, it is beneficial for a learning algorithm to adapt, near each point x , to the subspace that captures the local variability of the function f . We pose this task as kernel adaptation along a manifold with noise, and introduce Local EGOP learning, a recursive algorithm that utilizes the Expected Gradient Outer Product (EGOP) quadratic form as both a metric and inverse-covariance of our target distribution. We prove that Local EGOP learning adapts to the regularity of the function of interest, showing that under a supervised noisy manifold hypothesis, intrinsic dimensional learning rates are achieved for arbitrarily high-dimensional noise. Empirically, we compare our algorithm to the feature learning capabilities of deep learning. Additionally, we demonstrate improved regression quality compared to two-layer neural networks in the continuous single-index setting.

1 Introduction

Kernel methods are a powerful mechanism for studying machine learning algorithms. Many algorithms have leveraged the corresponding RKHS structure for efficient estimation of sufficiently regular functions [Wainwright, 2019], and functionals [Rao, 2014]. Further, many popular learning algorithms, such as certain neural network architectures and random forests, have been shown to asymptotically correspond to carefully chosen kernels [Jacot et al., 2018, Scornet, 2016]. Thus, the process by which investigators select kernels tailored to problems of interest, known as kernel engineering, is of central importance [Belkin et al., 2018]. Beyond allowing for potential efficiency gains, kernel engineer-

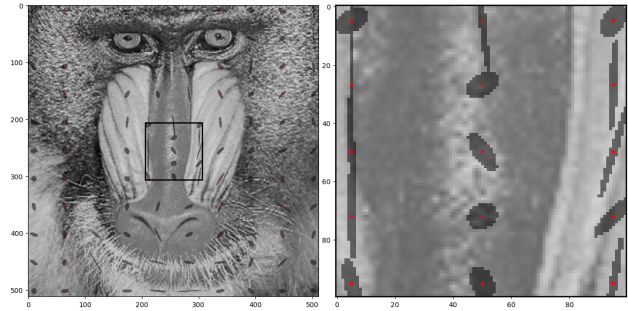


Figure 1: Localizations from Local EGOP Learning (Algorithm 1) centered at each of the highlighted points (in red) trained on a grayscale image of a mandrill [Bush 2021]. Here X is the pixel location and Y the grayscale value of the image. For visualization purposes the procedure was stopped early to enforce large localizations, and the 125 highest weight pixels are highlighted at each point. On the right the image is magnified to the highlighted region boxed-off on the left.

ing closely emulates the feature learning properties of deep neural networks.

Some objectives of kernel engineering include the design of specialized kernels suited to particular data structures ([Odene et al., 2005, Kondor and Jebara, 2003, Joachims, 1998, Chapelle et al., 1999, Barla et al., 2002, Vishwanathan et al., 2010], etc.), statistical principles ([Genton, 2001, Schölkopf et al., 1997, Osborne, 2010], etc.), and problems of interest (Gong et al. [2024], Kokot and Luedtke [2025], etc.). In regression settings, a classical approach is local feature learning, in which kernels are augmented by differential information at points of interest ([Schmid and Mohr, 1997, Wallraven et al., 2003, Lowe, 1999]). Earlier nonparametric methods developed a similar framework, with datasets being recursively partitioned to improve the quality of local fits [Heise, 1971, Breiman and Meisel, 1976, Friedman, 1979].

A modern incarnation of kernel engineering is *multi-*

index learning, particularly in the case of neural networks ([Mousavi-Hosseini et al., 2022, Boix-Adsera et al., 2023, Damian et al., 2023], etc.). This literature aims to show that the desirable properties of kernel engineering, such as data adaptivity and dimension reduction, are captured implicitly by certain machine learning models. Much work has been done in the *single-index* case, where the goal is to regress labels Y on features X when $f(x) := \mathbb{E}[Y|X = x]$ depends on x solely through their evaluation in a fixed direction v , via the quantity $v^T x$. It has been shown that two-layer neural networks not only learn this dependence, but also do so efficiently, leading to rapid increases in prediction quality ([Bietti et al., 2022, Abbe et al., 2024, Lee et al., 2024], etc.). Recent results indicate that these same benefits carry over to the multi-index setting for models trained via SGD [Damian et al., 2023, Arnaboldi et al., 2024].

In this paper, we generalize multi-index learning, introducing a new setting we call *continuous-index learning (CIL)*. Rather than encoding the dependence of x through the action of a low-rank matrix V , $f(x) = g(Vx)$, we allow V_x to be a continuously varying affine map, $f(x) = g(V_x x)$. Our window into this setting is via the *supervised noisy manifold hypothesis*, where we assume that the features X are concentrated about a d -dimensional manifold \mathcal{M} , and $f(x) = g(\pi(x))$ for $\pi(x) := \operatorname{argmin}_{q \in \mathcal{M}} \|q - x\|$ the nearest point projection onto \mathcal{M} . For such data, the normal space \mathcal{N}_x represents a continuously varying uninformative subspace, that is, for η normal to \mathcal{M} at $p := \pi(x)$, $\|\eta\|$ sufficiently small, $f(x + \eta) = f(x)$. The tangent $\mathcal{T}_x = \mathcal{N}_x^c$ we refer to as the informative subspace. This feature structure is typical in manifold learning settings [Aamari and Levraud, 2018, Genovese et al., 2012, Kokot et al., 2025].

We approach this problem via kernel smoothing, $\hat{f}(x) = \sum_i w_i Y_i$, $w_i \propto k(\|x - X_i\|)$ for a rbf k . By introducing a Mahalanobis metrization $k(\|M^{1/2}(x - X_i)\|)$, we seek to emulate the local multi-index structure of a continuous-index outcome. In particular, if M can be selected to degenerate along the normal then the weights will decay primarily along the informative tangent direction, leading to estimation rates scaling with the intrinsic manifold dimension d . Without a priori knowledge of the manifold \mathcal{M} , we develop a recursive procedure we call Local EGOP Learning, which iteratively refines the metric M by pooling coarse differential information estimated from the observed data.

Our method bears particular resemblance to “kernel steering”, which was developed in the image processing literature [Takeda et al., 2007] (see also the follow-up paper [Takeda et al., 2008]). The goal of kernel steering is to allow the kernel size and shape to change in a data-dependent way, adapting not only to sample

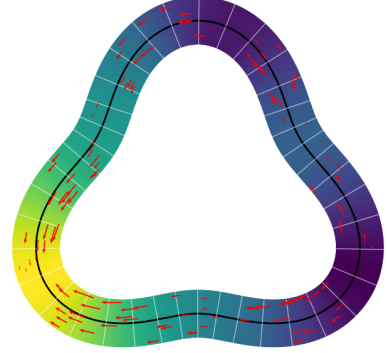


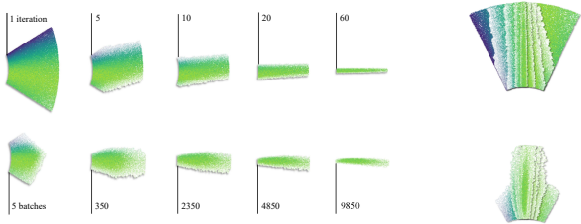
Figure 2: Supervised noisy manifold data in \mathbb{R}^2 . In a neighborhood about a closed curve we overlay a heatmap of a function invariant to normal displacement. The curve is displayed in black, the normal spaces are highlighted in white, and red gradients are displayed at randomly sampled points, with lengths proportionate to the gradient magnitude.

location and density, but also to local features in the data. A special case of these data-adaptive kernels appears in conjunction with the popular bilateral filter in computer vision [Tomasi and Manduchi, 1998], [Elad, 2002]. In Takeda et al. [2007], they propose an iterative procedure that estimates gradients about a point of interest. These are then used to “steer” the kernel locally, adopting the empirical covariance of the gradients $\hat{\mathcal{L}}$ near the point of interest as a Mahalanobis distance for subsequent estimation. Applying this method to the Gaussian kernel gives the steering kernel

$$K_{h, \hat{\mathcal{L}}}(x_i - x^*) \propto \exp \left\{ -\frac{(x_i - x^*)^T \hat{\mathcal{L}}(x_i - x^*)}{2h^2 \mu^2} \right\},$$

which can then be used to estimate the function again and further refine the estimate of $\hat{\mathcal{L}}$. To the best of our knowledge, concrete guarantees have yet to be proven for this algorithm. This directional adaptation enables more effective denoising and image recovery, and is closely related to the expected gradient outer product (EGOP) $\mathcal{L}(\mu) := \mathbb{E}_\mu[\nabla f(X)\nabla f(X)^T]$ [Samarov, 1993, Hristache et al., 2001, Xia et al., 2002, Trivedi et al., 2014, Yuan et al., 2023]. Besides kernel steering, local EGOP metrizations have appeared sporadically in different literatures, with common goals being to accelerate learning tasks and learn efficient dimension reductions [Trivedi et al., 2014, Wu et al., 2010, Mukherjee et al., 2010].

Recently, a similar procedure proposed in works such as Radhakrishnan et al. [2022, 2025], Zhu et al. [2025] emphasizes the importance of the Average Gradient Outerproduct (AGOP), which is the empirical covariance matrix of the estimated gradients $\hat{\mathcal{L}}(P_n) := \frac{1}{n} \sum_{i=1}^n \hat{\nabla} f \hat{\nabla} f^T$. These papers demonstrate, both em-



(a) Localizations μ_i from Local EGOP (top) and neural Learning (top) and a deep neural network (bottom) work feature embedding (bottom).
 (b) Layered EGOP (top) and neural network (bottom) localizations.

Figure 3: Local EGOP Learning and a deep transformer architecture applied to data sampled from an annulus. Labels are generated with no dependence on the radius in the parameterization, with these values overlaid as a heatmap. About the point $x^* = (1, 0)$, points are displayed with opacity $w \propto \exp(-d(x^*, x_i)^2)$, where $d(\cdot, \cdot)$ is the AGOP Mahalanobis distance (top) and transformer feature embedding (bottom). Both regions are displayed after progressively many iterations/training batches.

pirically and theoretically, that this object is closely associated with the performance of simple neural networks, and that its inclusion in a kernel machine allows for estimation adaptive to the global regularity of functions of interest.

However, $\mathcal{L}(\mu)$ may generically be full rank, making procedures such as the aforementioned subject to the curse of dimensionality. The supervised noisy manifold hypothesis is exactly such an example. Generically, $\cup_{x \in \mathcal{M}} \mathcal{T}_x = \mathbb{R}^D$, the full ambient space, hence globally all subspaces may be informative. Only locally will the EGOP degenerate, necessitating μ appropriately concentrate about the point of interest x^* . We study this through the lens of Gaussian localizations, $\mu = N(x^*, \Sigma)$. The covariance Σ and the Mahalanobis distance M have inverted proclivities, as where M seeks to degenerate along the normal, $\mathcal{L}(\mu)$ is most degenerate for Σ aligned with the normal. This is no coincidence, as upon selecting k Gaussian, smoothing with weights $\propto k(M^{1/2}(X_i - x^*))$ corresponds to an average with respect to $\mu = N(x^*, M^{-1})$.

We formally link these objects in Section 3, developing a rigorous framework to assess the contribution of anisotropy to learning rates for kernel estimators. In sections 4 and 5, we demonstrate how optimizing the corresponding bias-variance trade-off naturally leads to the Local EGOP Algorithm, a recursive procedure reminiscent to the methods proposed in Takeda et al. [2007], Radhakrishnan et al. [2022]. Finally, in section

6, we show that this method leads to adaptive regression guarantees for both noisy manifold and generic data. We support the theoretical results with numerical examples illustrating our claims in Section 7, and discuss further directions of research in Section 8.

2 Notation

We refer to the population distribution of our feature vectors $X \in \mathbb{R}^D$ as P , and its empirical distribution as P_n . We assume P has bounded C^1 density with respect to the Lebesgue measure on \mathbb{R}^D . When invoking the noisy manifold hypothesis, we denote by \mathcal{M} the base manifold of dimension d , by π the nearest point projection onto the manifold, and by \mathcal{T}_x and \mathcal{N}_x the tangent and normal spaces, respectively, at point $p := \pi(x) \in \mathcal{M}$. For π to be well-defined, we further assume that X lies within the reach of \mathcal{M} Federer [1959] almost surely. The labels Y are assumed to be of the form $Y_i = f(X_i) + \varepsilon$ for ε_i iid, mean zero, and finite 4th moment. We assume that $f \in C^4$, bounded with uniformly bounded derivatives. We reserve μ to refer to a localization or target distribution of data appropriately concentrated about the point of interest x^* with covariance Σ . We assume a uniform cap for the covariance, $\|\Sigma\| \leq \zeta < \infty$. We denote by $\langle \cdot, \cdot \rangle_F$ the Frobenius inner product. This work centers around the EGOP, $\mathcal{L}(\mu) := \int \nabla f(x) \nabla f(x)^T d\mu$, and its empirical counterpart the AGOP, $\hat{\mathcal{L}}(w) := \sum_i w_i \hat{\nabla} f \hat{\nabla} f^T$, for some estimator $\hat{\nabla} f$ of the gradient. By k , we denote a second-order kernel, satisfying typical assumptions in the nonparametric statistics literature, see for example Tsybakov [2009][Chapter 1]. In Section 3, we specialize results to the Gaussian kernel $k(\|x\|) \propto \exp(-\|x\|^2)$, but we discuss the general setting in Appendix B.1.4.

3 Bias Control via EGOP

In this section, we develop a theoretical framework for adaptive kernel machines. Define the empirical kernel estimator for predicting the value of f at x^* by

$$\hat{P}_M(f) := \frac{1}{\hat{C}_M} \frac{1}{n} \sum_{i=1}^n k(\|M^{1/2}[X_i - x^*]\|/\sqrt{2}) Y_i, \quad (1)$$

$$\hat{C}_M := \frac{1}{n} \sum_{i=1}^n k(\|M^{1/2}[X_i - x^*]\|/\sqrt{2}), \quad (2)$$

where the $D \times D$ matrix $M \succeq 0$ is a Mahalanobis metric to be learned. Its continuous counterpart is

$$P_M(f) := \frac{1}{C_M} \int k(\|M^{1/2}[y - x^*]\|/\sqrt{2}) f(y) dP(y), \quad (3)$$

$$C_M := \int k(\|M^{1/2}[y - x^*]\|/\sqrt{2}) dP(y). \quad (4)$$

To assess the quality of this predictor, we can measure its bias $\int (P_M(f) - f)^2 d\mu$ on a target distribution μ . Our key insight is that, when M and μ are chosen in correspondence, the bias can be related to a Dirichlet form in terms of the EGOP. To make this explicit, we introduce the EGOP-form

$$W(\mu) := \int \nabla f^T \Sigma(\mu) \nabla f d\mu = \text{tr}(\mathcal{L}(\mu) \Sigma(\mu)). \quad (5)$$

Lemma 1 (Poincaré Inequality). *Let $M_t \succeq 0$, and set $\mu_t = N(0, M_t^{-1})$. Then,*

$$\int (P_{M_t}(f) - f)^2 d\mu_t = O(W(\mu_t)).$$

Thus, if the anisotropic metric M_t is such that the variation of f around x^* , given by $\mathcal{L}(\mu_t)$, and the variance of x itself, given by $\Sigma(\mu_t)$, are close to low-rank and orthogonal, then the bias of the kernel estimator (3) is controlled by $W(\mu_t) = \langle \mathcal{L}(\mu_t), \Sigma(\mu_t) \rangle_F$, and will be nearly 0. Of critical importance are the first and second moments of the target distribution μ , motivating our Gaussian convention, although Gaussianity is not essential to achieve the desired bound. We note that this general structure, of metrizing by the inverse covariance, appears in disparate literatures, from classical local feature estimators [Schmid and Mohr, 1997], to VAEs [Chadebec and Allassonnière, 2022], and Langevin preconditioning [Cui et al., 2024].

We now seek to control the variance of the finite sample estimator \hat{P}_M of f at x^* .

Lemma 2 (Variance). *Let $M_t \succeq 0$ and set $\Sigma_t = M_t^{-1}$, $\mu_t = N(x^*, \Sigma_t)$. Then $\mathbb{E} \left[(\hat{P}_{M_t}(f) - P_{M_t}(f))^2 \right] = O(1/(n\sqrt{\det \Sigma_t}))$.*

Combining these bounds yields our fundamental error rate.

Theorem 1 (Local MSE). *Let $M_t \succeq 0$, and set $\Sigma_t = M_t^{-1}$, $\mu_t = N(x^*, \Sigma_t)$. Then,*

$$\mathbb{E} \left[\int (\hat{P}_{M_t}(f) - f)^2 d\mu_t \right] = O \left(\frac{1}{n\sqrt{\det \Sigma_t}} + W(\mu_t) \right).$$

In particular, if $W(\mu_t) = O(t)$ and $\det \Sigma_t = O(t^q)$ then the asymptotic learning rate is

$$\mathbb{E} \left[\int (\hat{P}_{M_t}(f) - f)^2 d\mu_t \right] = O \left(n^{-\frac{1}{1+q/2}} \right).$$

Thus, if we design a sequence $\{t_i\}_{i \in \mathbb{N}}$, with $t_i \rightarrow 0$, such that M_{t_i} and μ_{t_i} are updated recursively based on their values up to t_{i-1} and $\frac{1}{n\sqrt{\det \Sigma_{t_{i-1}}}} + W(\mu_{t_{i-1}}) \rightarrow 0$, the kernel estimator $\hat{P}_{M_{t_{i-1}}}$ is consistent and its rate is controlled by the convergence rate of W and M .

Algorithm 1: Local EGOP Learning

Input: Data $\{(X_i, Y_i)\}_{i=1}^n$, target x^* , subsample size m , iterations T , bandwidths $\{t_i\}$, $\beta > 0$, scale $\alpha > 0$.
Output: Best estimate $\hat{f}(x^*)$.
Hyperparameters: $M_0 \leftarrow I/\alpha$.

```

1 bestMSE  $\leftarrow \infty$ ,  $\hat{f}_{\text{best}}(x) \leftarrow \emptyset$ ;
2 for  $i = 0$  to  $T - 1$  do
     $\triangleright$  Compute global weights at  $x^*$ 
    3  $w_j \propto \exp(-(X_j - x^*)^T M_i (X_j - x^*))$ ,  $j = 1, \dots, n$ ;
    4 Normalize  $w$ , subsample  $S \subset \{1, \dots, n\}$ ,  $|S| = m$ 
        with probs  $w$ ;
     $\triangleright$  Leave-One-Out Local regressions at each
    5  $j \in S$ 
    for  $j \in S$ , do
        Fit weighted local linear regression centered at
         $X_j$  (weights from metric  $M_i$ ), data point
         $(X_j, Y_j)$  excluded;
        6 Obtain  $\hat{\nabla} f[j]$  and  $\hat{f}[j]$ ;
     $\triangleright$  Aggregate statistics
    7  $L_i \leftarrow \sum_{j \in S} w_j \hat{\nabla} f[j] \hat{\nabla} f[j]^T$ ;
    8  $\widehat{\text{MSE}}_i \leftarrow \sum_{j \in S} w_j (Y_j - \hat{f}[j])^2$ ;
    9 if  $\widehat{\text{MSE}}_i < \text{bestMSE}$  then
        Estimate  $\hat{f}(x^*)$  via local regression centered at
         $x^*$ ;
        10 bestMSE  $\leftarrow \widehat{\text{MSE}}_i$ ,  $\hat{f}_{\text{best}}(x^*) \leftarrow \hat{f}(x^*)$ ;
     $\triangleright$  Metric update: set  $\beta = 1$  if  $i = 0$ ,  $\beta < 1$ 
    otherwise
    11  $M_{i+1} \leftarrow (\beta L_i + (1 - \beta) L_{i-1})$ ;
    12  $M_{i+1} \leftarrow M_{i+1}/[t_{i+1} \text{tr}(M_{i+1})]$ ;
    13 return  $\hat{f}_{\text{best}}(x)$ 

```

4 The Local EGOP Algorithm

In this section, we introduce the Local EGOP Learning algorithm, detailed in Algorithm 1. The theoretical motivation for this iterative scheme is presented in Section 5. The algorithm iteratively metrizes a kernel by an AGOP, leveraging this operator to assign weights to points neighboring x^* .

The time complexity of the method is $O(T((m+2)nD^2 + (m+1)D^3))$, with memory overhead $O(nD^2 + m^2D^2 + mD^3)$.

Incorporated into this algorithm is a one-step look-back (step 13) facilitated through $\beta \in (0, 1)$. This is essential to improve stability, as discussed in Example 2. In practice, one might choose hyper-parameters β, T , as well as the schedule $\{t_i\}$ via cross-validation. Additionally, for computational reasons, we normalize M_i by its trace (step 14) before applying the scaling factor. This has little impact asymptotically, as the trace converges to the leading gradient eigenvalue of the EGOP, making this normalization effectively equivalent to normalization by a constant scalar. However, it

serves a practical benefit by stabilizing initial iterates, setting the scale of the metric to the predefined rate $1/t_i$. Note that while the optimal number of iterations is dimension dependent, as argued in Theorems 1 and 3, our algorithm incorporates a Leave-One-Out style validation loop (step 10) for adaptive stopping.

5 Recursive Kernel Learning as Variance Minimization

We will now show how recursive kernel learning, combined with our basic kernel bounds, constitutes a greedy variance reduction strategy. Intuitively, the goal is to induce anisotropy in the kernel, stretching or steering it to include additional low-bias points that would otherwise be discarded with a RBF. The inclusion of these additional high-quality points is exactly a reduction of variance, as including more data results in tighter concentration to the mean for a local averaging estimator.

We now make precise how one can arrive at this by leveraging Theorem 1. Ideally, as spelled out in this result, we would like to select μ_t such that $W(\mu_t) \rightarrow 0$, and that $\det \Sigma(\mu_t)$ is as large as possible. In other words, if we specify the rate $W(\mu_t) = \text{tr}[\mathcal{L}(\mu_t)\Sigma(\mu_t)] = t \rightarrow 0$, it would be optimal to select the largest possible region that achieves this bias, meaning we would like to select

$$\mu_t = \text{argmax}_{\text{tr}[\mathcal{L}(\mu_t)\Sigma(\mu_t)] \leq t} \log \det \Sigma(\mu_t).$$

This, however, cannot be solved, as we lack precise knowledge of the function of interest f . Moreover, $\text{tr}[\mathcal{L}(\mu_t)\Sigma(\mu_t)] \leq t$ presents a challenging feasible set, as it is posed over a space of probability distributions, thus making it non-Euclidean. Our Gaussian ansatz reduces the problem to optimizing a finite parameterization, however this still presents a non-convex optimization.

This leads us to the following discretized relaxation of the problem. Let $t_i \rightarrow 0$ and set $\mu_0 = N(x^*, \alpha I)$, an isotropic initialization. If we compute the initial $\hat{\mathcal{L}}(\mu_0)$, we may hope that, as long as μ_1 represents a sufficiently comparable distribution, $\hat{\mathcal{L}}(\mu_0) \approx \hat{\mathcal{L}}(\mu_1)$. Thus, we can compute

$$\Sigma_1 = \text{argmax}_{\text{tr}[\hat{\mathcal{L}}(\mu_0)\Sigma] \leq t_1} \log \det \Sigma = t_1 \hat{\mathcal{L}}(\mu_0)^{-1} / D.$$

This yields $\mu_1 = N(x^*, \Sigma_1)$, and the corresponding kernel estimator is metrized by $\Sigma_1^{-1} \propto \hat{\mathcal{L}}(\mu_0)$. Repeating this, we have a recursive kernel learning algorithm, as we summarize below.

Proposition 1 (Alternating Minimization). *Let $t_i \rightarrow 0$, fix Σ_0 , $\mu_i = N(x^*, \Sigma_i)$, $\hat{\mathcal{L}}_i := \hat{\mathcal{L}}(\mu_i) := \int \hat{\nabla} f \hat{\nabla} f^T d\mu_i$, and construct $\hat{\nabla} f = \hat{P}_{\Sigma_i^{-1/2}}(f)$. Define the recursive kernel learning algorithm $\Sigma_{i+1} =$*

$t_{i+1} \hat{\mathcal{L}}_i^{-1} / D$. Then, equivalently,

$$\begin{aligned} \Sigma_{i+1} &= \text{argmax}_{\text{tr}[\hat{\mathcal{L}}(\mu_i)\Sigma] \leq t_{i+1}, \Sigma \succeq 0} \log \det \Sigma \\ &= \text{argmin}_{\text{tr}[\hat{\mathcal{L}}(\mu_i)\Sigma] = t_{i+1}, \Sigma \succeq 0} \text{tr}[\hat{\mathcal{L}}(\mu_i)\Sigma] + \frac{1}{n\sqrt{\det \Sigma}}. \end{aligned} \quad (6)$$

We note that in Algorithm 1, we use local linear regression to better fit into the EGOP estimation loop. We expect that a suitable extension of our theory is possible for higher-order polynomials, allowing for more complex local regressions in Algorithm 1. See Section 8 for further details.

From this framework we have developed, it is clear that there are many possible schemes to optimize the bias-variance trade-off, and we discuss this in more detail in Section 8. We choose to focus on this alternating optimization scheme because it strongly resembles algorithms present in the existing literature, and is simple to implement.

6 Guarantees

In this section, we demonstrate concrete theoretical guarantees for estimation via Local EGOP Learning. In our theory, we do not consider the problem of EGOP estimation, and instead consider an iterative scheme in which we can query an oracle for the EGOP associated to a particular choice of covariance. For our experiments, we compute empirical AGOPs fit via the proposed iterative estimation procedure, leading to sharp estimation quality. We leave it to future work to close this theoretical gap, although we discuss it in greater depth in Appendix C. See Appendix B for proofs of all following arguments.

6.1 Taylor Expansion

Up to this point, our prevailing perspective is that the target distributions μ matter up to their first and second moments, passing the optimization problem from the space of measures to the PSD cone, and informing a Gaussian relaxation. We close the loop to EGOP estimation by additionally Taylor expanding $\mathcal{L}(\mu)$ up to second order, reducing the proposed iteration scheme entirely to a recurrence in Σ .

Lemma 3 (Generic Taylor Expansion). *Let $\mu = N(x^*, \Sigma)$, $g = \nabla f(x^*)$, and $H = \nabla^2 f(x^*)$. Then there exist $T : \mathbb{R}^{D \times D} \rightarrow \mathbb{R}^D$, $R : \mathbb{R}^{D \times D} \rightarrow \mathbb{R}^{D \times D}$, $C_T \geq 0$, and $C_R \geq 0$ such that for any $A \succeq 0$, $\|T(A)\| \leq C_T \|A\|$, $\|R(A)\| \leq C_R \|A\|^2$, and*

$$\mathcal{L}(\mu) = gg^T + H\Sigma H + gT(\Sigma)^T + T(\Sigma)g^T + R(\Sigma).$$

Define $T_g(\Sigma) := gT(\Sigma)^T + T(\Sigma)g^T$. Our goal is to

analyze

$$\begin{aligned}\Sigma_{i+1} &= t_{i+1}(\beta\mathcal{L}(\mu_i) + (1-\beta)\mathcal{L}(\mu_{i-1}))^{-1} \\ &= t_{i+1}(gg^T + \beta[H\Sigma_iH + T_g(\Sigma_i) + R(\Sigma_i)], \\ &\quad + (1-\beta)[H\Sigma_{i-1}H + T_g(\Sigma_{i-1}) + R(\Sigma_{i-1})])^{-1}.\end{aligned}\quad (7)$$

We initialize this recurrence with the isotropic choice $\Sigma_0 = \alpha I$, $\Sigma_1 = t_1\mathcal{L}(\mu_0)^{-1}$, $\Sigma_2 = t_1\mathcal{L}(\mu_1)^{-1}$, then apply momentum following this step.

6.2 Full Rank Hessian

We begin our analysis with the generic setting, where H is full-rank. In this setting, the Taylor expansion of $\mathcal{L}(\mu)$ is dominated by a rank 1 matrix gg^T and a linear term $H\Sigma H$, which combine to yield a full rank matrix. We show that Local EGOP Learning results in a marked efficiency gain over generic isotropic kernel methods. Indeed, we argue that $g^T\Sigma_i g = \Theta(t_i)$, while for $v \perp g$, $v^T\Sigma_i v = \Theta(\sqrt{t_i})$, thus achieving a second-order anisotropy. The noisy manifold setting implies a rank deficiency of H , and we will show in the next section how this leads to further efficiency gains.

Example 1 (Scalar Recurrence). Fix a schedule for $t_i \rightarrow 0$ that is no faster than geometric, so that t_{i+1}/t_i is larger than a fixed threshold. We investigate a considerable reduction of the problem, the one dimensional recurrences

$$a_{i+1} = \frac{t_{i+1}}{\beta a_i + (1-\beta)a_{i-1}}, \quad (8)$$

$$b_{i+1} = \frac{t_{i+1}}{c + \beta b_i + (1-\beta)b_{i-1}}. \quad (9)$$

It is easy to see that $b_i = O(t_i)$, as if b_i decays at all, then we have $b_i = t_i/c + o(t_i)$. One can also readily observe, at least informally, the rate of decay of a_i . Assume that $a_i = \Theta(t_i^\zeta)$. By the recurrence relation, we then have $a_i = \Theta(t_i^{1-\zeta})$, hence these coincide at the second order anisotropy $\alpha = 1/2$. As our matrix recurrence is primarily given by a homogeneous part ($H\Sigma H$) plus a rank deficient constant part (gg^T), we argue in Appendix B that the b_i correspond well to the $g \times g$ block of Σ_i , and a_i to $g^\perp \times g^\perp$.

Example 2 (Momentum). We now take a moment to highlight the necessity of the momentum term $\beta > 0$. Consider, again, the sequence a_i from Example 1, and suppose we set $\beta = 1$. For convenience, let us assume $\sqrt{t_{i+1}} = \sqrt{t_i}r$, an exact geometric schedule. We reparameterize, writing

$$a_{i+1} = \frac{t_{i+1}}{a_i} \iff a'_{i+1} = \frac{1}{a'_i}$$

for $a'_i := \frac{a_i}{\sqrt{t_i}}$. Clearly, a'_i has no limit, as it simply oscillates wildly about 1. The remainder terms, as

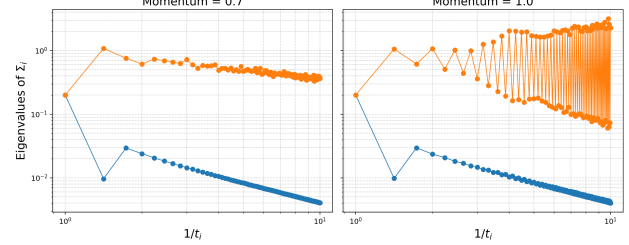


Figure 4: Comparison of the eigenvalue decay of Σ_i for Local EGOP Learning with and without momentum. On the left, we set $\beta = 0.7$, on the right $\beta = 1$ (no momentum). Without momentum, the second order eigenvalues are prone to wild oscillations.

well as the estimation error, make the $\sqrt{t_i}$ rate become unstable, leading to potential catastrophic failure. We demonstrate the resulting localizations with and without momentum in Figure 4.

This leads to the following result.

Theorem 2 (Second Order Anisotropy). *Let H be invertible and Σ_i satisfy the recurrence in equation 7, $\sqrt{t_i} = \alpha r^i$, $0 < r < 1$, $\beta > 0$. Then, for α sufficiently small, $g^T\Sigma_i g = \Theta(t_i)$, and for $v \perp g$, $v^T\Sigma_i v = \Theta(\sqrt{t_i})$. It follows that, selecting $i_n = \frac{4 \log n}{(D+5) \log(1/r)}$,*

$$\mathbb{E} \left[\int (\hat{P}_{\Sigma_{i_n}}(f) - f)^2 d\mu_{i_n} \right] = O \left(n^{-\frac{4}{D+5}} \right).$$

Compared to a vanilla 0-order local polynomial estimator, this method nearly squares the asymptotic error, effectively cutting the effective dimension in half for D large. In our theory, we assume the initial localization has small covariance αI . In the resulting application of Lemma 3, this results in an explicit recurrence up to a higher-order remainder. While a useful theoretical construct, this is not necessary empirically, and we leave it to future research for a complete analysis of the iteration stability.

6.3 Noisy Manifold

In the noisy manifold setting we strengthen Lemma 4.

Lemma 4 (Noisy Manifold Taylor Expansion). *Let $g = \nabla f(0)$, $H = \nabla^2 f(0)$, $p = \pi(0)$, $\mathcal{T} := \mathcal{T}_p$, $\mathcal{N} := \mathcal{N}_p$, and T, R be as in Lemma 4. There exist non-negative constants C_N and $C_{\mathcal{T}N}$ such that, for all $A \succeq 0$,*

$$\|\pi_N R(A)\pi_N\| \leq C_N \|\pi_{\mathcal{T}} A \pi_{\mathcal{T}}\|^2, \quad (10)$$

$$\|\pi_{\mathcal{T}} R(A)\pi_N\| \leq C_{\mathcal{T}N} \|\pi_{\mathcal{T}} A \pi_N\|. \quad (11)$$

Additionally, $\text{rank}(H) \leq 2d$.

We will leverage this weak orthogonal dependence to show that the distribution μ elongates along the space

\mathcal{N}_{x^*} orthogonal to the manifold. However, while the function is constant on this fiber, its gradient is not. Indeed, we are only guaranteed that the gradient remains tangent. Due to the effects of curvature, $\nabla f(p+v)$ may shrink or grow along different coordinate directions. We characterize this precisely as follows.

Lemma 5 (Gradient Geometry). *Let $p \in \mathcal{M}$, $\eta \in \mathcal{N}_p$, $\|\eta\| < \tau$, τ the reach of \mathcal{M} . Then,*

$$\nabla f(p+\eta) = (I - S_p(\eta))^{-1} \nabla f(p).$$

In particular, for any such η , there exists a subspace $\text{Null} = \text{Null}_\eta$ of dimension at least $D - 2d$ such that for any $v, z \in \text{Null}$, $\nabla f(p+\eta+v) = \nabla f(p+\eta)$, $\nabla^2 f(p+\eta+v)z = 0$.

These geometric implications allow us to further adapt Lemma 4 to our geometry.

Corollary 1 (Shifted Taylor). *Let $x^* = p + \eta$, $v \in \text{Null}_\eta$. Define μ_v as the measure $\mu = N(x^*, \Sigma)$ conditioned on $\pi_{\text{Null}}[X - x^*] = v$, i.e. the draws where the Null component is fixed at v . Let Σ_v be the covariance of this distribution. Then,*

$$\mathcal{L}(\mu_v) = gg^T + H_v \Sigma_v H_v + g T_v(\Sigma_v)^T + T_v(\Sigma_v) g^T + R_v(\Sigma_v)$$

where $\text{Null} \subseteq \text{nullspace}(H_v)$, $\sup_{v \in \text{Null}} \|R_v(A)\| \leq C_{\text{Null}} \|A\|^2$, $T_v(A) \leq C_{\text{Null}} \|A\|$ for a uniform constant C_{Null} , and H_v, T_v, R_v are continuous in v , Lipschitz in $\|A\|$.

This allows us to perform an iterated integration, freezing the Taylor expansion along this shifted base point while preserving the fundamental first order behavior. To simplify our argument we assume that the covariance cap ζ is small, allowing a simple reduction of the dynamics to the non-degenerate case. This greatly streamlines the analysis, although we do not believe it is fundamental to the convergence.

Theorem 3 (Intrinsic Learning Rate). *Assume that $D \geq 2d$ and $\text{rank}(H) = 2d$. Let Σ_i satisfy the recurrence in equation 7, $\sqrt{t_i} = \alpha r^i$, $0 < r < 1$, $\beta > 0$. Then, for $\alpha = \zeta$ sufficiently small, $g^T \Sigma_i g = \Theta(t_i)$, for $v \in \text{Null}$, $v^T \Sigma_i v = \Theta(1)$, and for $\eta \in \text{Null}^\perp \cap g^\perp$, $\eta^T \Sigma_i \eta = \theta(\sqrt{t_i})$. It follows that, selecting $i_n = \frac{4 \log n}{(2d+5) \log(1/r)}$,*

$$\mathbb{E} \left[\int (\hat{P}_{\Sigma_{i_n}}(f) - f)^2 d\mu_{i_n} \right] = O \left(n^{-\frac{4}{2d+5}} \right).$$

Rather than fully denoising the manifold, our analysis reveals that the manifold tangent, as well as the normal vectors that do not fall in Null , are subject to the same second-order anisotropy as observed in the full rank setting. These compose precisely those directions in which the gradient varies at first order, leaving only the

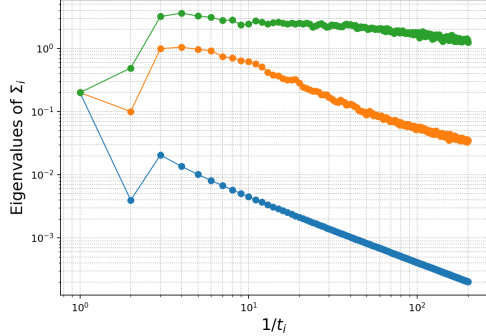


Figure 5: Eigenvalue decay of Σ_i with Local EGOP Learning applied to data satisfying the noisy manifold hypothesis about S^2 . The orthogonal exhibits light decay, approaching second order anisotropy asymptotically.

inactive subspace where the linearization is preserved. Practically, the resulting rate is comparable to that of a standard estimator applied to a completely denoised manifold, as this method yields an effective dimension of $d + 1/2$.

Example 3 (Spheres). Built into Theorem 3 are assumptions on the ambient dimension and derivatives of f . The sphere S^{D-1} is a typical toy example, however $D \geq 2(D-1)$ fails for $D \geq 3$. In these settings, the hessian has the form

$$H = \begin{bmatrix} T & b \\ b^T & 0 \end{bmatrix}$$

in the $\mathcal{T} \times \mathcal{N}$ basis. Thus the noisy manifold hypothesis only guarantees that a single entry of the Hessian is 0. Hence, $\pi_{g^\perp} H \pi_{g^\perp}$ is generically full rank, driving second order anisotropy along the tangent and orthogonal, as demonstrated in Figure 5.

Example 4 (Multi-Index Learning). When the underlying manifold \mathcal{M} is flat, the supervised noisy manifold hypothesis reduces to a multi-index setting. The key distinction is that displacement away from the manifold not only preserves the function value, but also all higher order function derivatives. In particular, the Hessian has rank no more than d , the active index dimension, and the Hessian column space is shared across the distribution.

Thus, when performing expansions such as Corollary 1, the orthogonal has no contribution to the EGOP, leading to implicit dimension reduction. In particular, this yields a learning rate of $(d + 1)/2$.

7 Experiments

We provide the following simulations to empirically justify our theoretical results. First, expanding on the

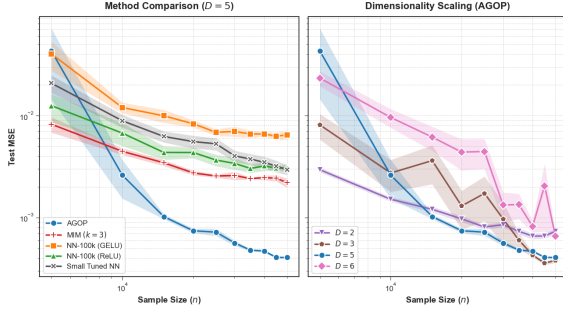


Figure 6: (Left) Comparison of Local EGOP Learning to the performance of a two-layer neural network architectures trained on helical data in ambient dimension $D = 5$. (Right) Local EGOP Learning trained on helical data in various ambient dimensions D .

noisy manifold setting, we show how the regression error rates of Local EGOP Learning remain invariant to the injection of high-dimensional noise. We demonstrate that two-layer neural networks are not able to efficiently learn in the noisy manifold setting, with a sharp decrease in performance compared to Local EGOP Learning. Next, we compare the performance of our method to that of a deep neural network on toy data. In particular, we show how the feature embeddings produced by transformers trained on a simple example are qualitatively similar to the localizations generated by our procedure. Finally, we apply this procedure to estimate backbone angles in Molecular Dynamics (MD) data, where we leverage the noisy manifold structured data to improve prediction quality.

In our simulations, we consider helical data, parameterized by a curve $\theta(t) = (\sin(t + w_1), \cos(t + w_1), \sin(t + w_2), \cos(t + w_2), \dots, g(t))$, where $g(t) = t$ is a linear term included if D is odd dimensional, and the w_i are constant offsets taken as a mesh from 0 to 2π . We rescale this data by a constant τ , then contaminate it with uniform orthogonal noise of radius r . In our simulations, we set $\tau = 0.8$, $r = 0.5$, and sample t from 0 to 2π . See Figure 7a for a visualization. For the outcomes y , we generate a third-degree polynomial with coefficients uniformly sampled from $(-3, 3)$, then evaluate it at the projection point onto $\theta(t)$.

We relegate details for the evaluation and fitting of each method to Appendix A.

7.1 Learning Rate

We generate helical data in a variety of dimensions, testing the Local EGOP Learning algorithm. As seen in Figure 6, the asymptotic learning rate has little dimensional dependence. However, error scaling depends strongly on whether D is even or odd, and this is be-

cause the underlying manifold changes in these settings, although its intrinsic dimension does not.

7.2 Two-layer Neural Network

We assess a variety of two-layer neural network architectures, with implementation and training explained in detail in Appendix A.

Helical data provides a rich experimental setting to compare Local EGOP Learning to two-layer neural networks. It is not only continuous single-index, it is multi-index 2 for D even, and 3 for D odd. Further, by construction it is well-approximated by a low intrinsic dimensional manifold, a typical setting for accelerated learning rates (Kiani et al. [2024], Liu et al. [2021], etc.).

Unsurprisingly, as demonstrated in Figure 6, the two-layer neural networks readily adapt to the multi-index data structure. For $D = 5$, the overparameterized ReLU network achieves comparable error to a multi-index architecture pre-specified to learn a 3-dimensional subspace. However, Local EGOP Learning vastly reduced the error for moderate to large sample sizes. This suggests that no architecture was able to fully adapt to the intrinsic continuous single-index structure.

7.3 Feature Learning

In this section, we compare the local feature learning capabilities of a deep transformer-based neural network [Gorishniy et al., 2023] to Local EGOP Learning. We consider data generated from a 1-sphere under the supervised noisy manifold hypothesis. On this simple dataset, both algorithms result in nearly complete denoising of the data, as shown in Figures 3a and 3b. In Appendix A, we provide additional unsupervised embeddings for comparison.

7.4 Predicting the backbone angles in Molecular Dynamics (MD) data

Our final example comes from the analysis of molecular geometries. The raw data consist of X, Y, Z coordinates for each of the N_a atoms of a molecule, which, due to interatomic interactions, lie near a low-dimensional manifold [Das et al., 2006]. While the governing equations of the simulated dynamics are unknown, for small organic molecules, certain backbone angles [Das et al., 2006] have been observed to vary along the aforementioned low-dimensional manifold. Specifically, for the malonaldehyde molecule, the two backbone angles denoted $\tau_{1,2}$ are shown in Figure 7b. We used a subsample of molecular configurations of size $n = 10^4$ from the MD simulation data of Chmiela et al. [2017] as input data. The configuration data, pre-processed as in Koelle et al.

[2022], consists of $D = 50$ dimensional vectors and lie near a 2-dimensional surface with a torus topology (see Figure 7b). On a hold-out set of 500 test points, Local EGOP Learning yields an MSE of 0.00043, compared to 0.012 for Gaussian kernel Nadaraya-Watson with cross-validated bandwidth selection.

8 Discussion and Future Work

The primary contribution of this work is to establish a rigorous basis for the study of recursive kernel machines that localize about points of interest. We leverage this framework to verify that Local EGOP Learning achieves desirable learning rates in model settings. Of particular importance is our introduction of continuous index learning, formalized by the supervised noisy manifold hypothesis, under which anisotropy about the orthogonal is achieved under appropriate non-degeneracy assumptions. Our algorithm is most similar to the heuristic Takeda et al. [2007], hence we believe that the present framework can be extended to analyze this algorithm, too. Local EGOP takes its name from Radhakrishnan et al. [2022], with the key distinction being that the AGOP is averaged over the localized region μ_i rather than the entire data distribution P_n .

We demonstrate the efficacy of this algorithm, qualitatively when compared to a transformer architecture, and quantitatively on high dimensional continuous single-index data. The theoretical framework developed in this work opens many avenues for future study. In addition to the open problems this investigation has raised, our approach is conducive to a variety of strategies that may further improve the stated results. We mention several of the most relevant directions.

For one, we can consider optimizing the objective

$$\text{tr}[\mathcal{L}(\mu_t)\Sigma(\mu_t)] + \frac{1}{n\sqrt{\det \Sigma(\mu_t)}}$$

in a variety of ways. Working with a second order relaxation, one may seek to optimize the covariance gradually, such as by a gradient-based method. Alternatively, motivated by Proposition 1, one can show that this ratio is minimized by a distribution μ_t such that $\Sigma(\mu_t) = t\mathcal{L}(\mu_t)^{-1}/D$. Differentiating, this yields a differential equation

$$\partial_t \mathcal{L}(\mu_t)\Sigma(\mu_t) + \mathcal{L}(\mu_t)\partial_t \Sigma(\mu_t) = I/D$$

which may be amenable to analysis, particularly in the Gaussian setting. However, it may also be fruitful to drop both this assumption and the covariance relaxation. One promising direction is to view $W(\mu_t)$ and $\Sigma(\mu_t)$ as functionals, and to then optimize the ratio using the Wasserstein gradient flow [Ambrosio

et al., 2006] or other methods that operate at the distribution level. In particular, this would allow for non-ellipsoidal localizations, potentially allowing for improved learning rates in settings where the level-set is curved. A fundamental hurdle for any of these approaches is that, generally, the EGOP-form can only upper bound localization-induced bias, and the resulting bound is not always sharp.

Many basic questions have been left for future research. As discussed in Appendix C, in the context of Local EGOP Learning, the problem of EGOP estimation is left open. Algorithm 1 is slow, requiring many local linear regressions at each iteration. We presented this simple algorithm for clarity, and many practical improvements can be made to improve its performance, particularly when multiple data points are queried for prediction. Furthermore, simple modifications to the algorithm would yield gains in statistical efficiency. Higher-order local polynomial regression can be performed for function estimation. This would improve theoretical guarantees by accounting for more general smoothness patterns in the function of interest, but it may also inform more complex localization procedures. Gaussian localizations are quadratic in nature, and so a more generic formulation may yield increased adaptivity.

Importantly, Local EGOP Learning is based firmly on a MSE formulation of regression, restricting its utility to ℓ_2 loss. It is unlikely that this method can be applied directly to problems such as classification or image generation. This leaves open how an appropriate adaptation should be formulated in these settings. Additionally, a formal analysis comparing procedures such as Local EGOP Learning to modern neural network architectures is merited. In particular, while we do not expect an exact replication of behavior, the Local EGOP ansatz, which asserts that learned features ought to spread locally inversely proportionate to the EGOP, may inform further study of these learning algorithms, or lead to improvements in the design of model architectures.

Acknowledgements

The authors would like to thank Misha Belkin for the initial suggestion of comparing Local EGOP Learning to the performance of two-layer neural networks, and Brennan Dury for suggestions and experiments related to earlier conceptions of this research.

References

Eddie Aamari and Clément Levraud. Non-asymptotic rates for manifold, tangent space, and curvature

estimation, 2018. URL <https://arxiv.org/abs/1705.00989>.

Emmanuel Abbe, Enric Boix-Adsera, and Theodor Misiakiewicz. The merged-staircase property: a necessary and nearly sufficient condition for sgd learning of sparse functions on two-layer neural networks, 2024. URL <https://arxiv.org/abs/2202.08658>.

L. Ambrosio, N. Gigli, and G. Savare. *Gradient Flows: In Metric Spaces and in the Space of Probability Measures*. Lectures in Mathematics. ETH Zürich. Birkhäuser Basel, 2006. ISBN 9783764373092. URL https://books.google.com/books?id=Hk_wNp0sc4gC.

Luca Arnaboldi, Yatin Dandi, Florent Krzakala, Luca Pesce, and Ludovic Stephan. Repetita iuvant: Data repetition allows sgd to learn high-dimensional multi-index functions. *arXiv preprint arXiv:2405.15459*, 2024.

Dominique Bakry, Ivan Gentil, and Michel Ledoux. *Analysis and geometry of Markov diffusion operators*, volume 348. Springer Science & Business Media, 2013.

Annalisa Barla, Francesca Odone, and Alessandro Verri. Hausdorff kernel for 3d object acquisition and detection. In *Computer Vision—ECCV 2002: 7th European Conference on Computer Vision Copenhagen, Denmark, May 28–31, 2002 Proceedings, Part IV 7*, pages 20–33. Springer, 2002.

Mikhail Belkin, Siyuan Ma, and Soumik Mandal. To understand deep learning we need to understand kernel learning. In *International Conference on Machine Learning*, pages 541–549. PMLR, 2018.

Alberto Bietti, Joan Bruna, Clayton Sanford, and Min Jae Song. Learning single-index models with shallow neural networks. *Advances in neural information processing systems*, 35:9768–9783, 2022.

Enric Boix-Adsera, Eta Littwin, Emmanuel Abbe, Samy Bengio, and Joshua Susskind. Transformers learn through gradual rank increase. *Advances in Neural Information Processing Systems*, 36:24519–24551, 2023.

Leo Breiman and William S Meisel. General estimates of the intrinsic variability of data in nonlinear regression models. *Journal of the American Statistical Association*, 71(354):301–307, 1976.

Jeffrey Bush. C4l image dataset, 2021. URL <https://dx.doi.org/10.21227/bc9m-f507>.

Clément Chadebec and Stéphanie Allassonnière. A geometric perspective on variational autoencoders, 2022. URL <https://arxiv.org/abs/2209.07370>.

Olivier Chapelle, Patrick Haffner, and Vladimir N Vapnik. Support vector machines for histogram-based image classification. *IEEE transactions on Neural Networks*, 10(5):1055–1064, 1999.

Stefan Chmiela, Alexandre Tkatchenko, Huziel Sauceda, Igor Poltavsky, Kristof T. Schütt, and Klaus-Robert Müller. Machine learning of accurate energy-conserving molecular force fields. *Science Advances*, March 2017.

Ronald R Coifman and Stéphane Lafon. Diffusion maps. *Applied and computational harmonic analysis*, 21(1):5–30, 2006.

Tiangang Cui, Xin Tong, and Olivier Zahm. Optimal riemannian metric for poincaré inequalities and how to ideally precondition langevin dynamics. *arXiv preprint arXiv:2404.02554*, 2024.

Alex Damian, Eshaan Nichani, Rong Ge, and Jason D Lee. Smoothing the landscape boosts the signal for sgd: Optimal sample complexity for learning single index models. *Advances in Neural Information Processing Systems*, 36:752–784, 2023.

P. Das, M. Moll, H. Stamati, L.E. Kavraki, and C. Clementi. Low-dimensional, free-energy landscapes of protein-folding reactions by nonlinear dimensionality reduction. *Proceedings of the National Academy of Sciences*, 103(26):9885–9890, 2006.

Manfredo P Do Carmo. *Differential geometry of curves and surfaces: revised and updated second edition*. Courier Dover Publications, 2016.

Michael Elad. On the origin of the bilateral filter and ways to improve it. *IEEE Transactions on image processing*, 11(10):1141–1151, 2002.

Herbert Federer. Curvature measures. *Transactions of the American Mathematical Society*, 93(3):418–491, 1959.

Jerome H Friedman. A tree-structured approach to nonparametric multiple regression. In *Smoothing Techniques for Curve Estimation: Proceedings of a Workshop held in Heidelberg, April 2–4, 1979*, pages 5–22. Springer, 1979.

Nicolas Garcia Trillos. Variational limits of k-nn graph-based functionals on data clouds. *SIAM Journal on Mathematics of Data Science*, 1(1):93–120, 2019.

Christopher R. Genovese, Marco Perone-Pacifico, Isabella Verdinelli, and Larry A. Wasserman. Minimax manifold estimation. *Journal of Machine Learning Research*, 13:1263–1291, 2012. URL <http://dl.acm.org/citation.cfm?id=2343687>.

Marc G Genton. Classes of kernels for machine learning: a statistics perspective. *Journal of machine learning research*, 2(Dec):299–312, 2001.

Albert Gong, Kyuseong Choi, and Raaz Dwivedi. Supervised kernel thinning. *arXiv preprint arXiv:2410.13749*, 2024.

Yury Gorishniy, Ivan Rubachev, Valentin Khrulkov, and Artem Babenko. Revisiting deep learning models for tabular data. *Advances in neural information processing systems*, 34:18932–18943, 2021.

Yury Gorishniy, Ivan Rubachev, and Artem Babenko. On embeddings for numerical features in tabular deep learning, 2023. URL <https://arxiv.org/abs/2203.05556>.

David R Heise. Multivariate model building: The validation of a search strategy., 1971.

Marian Hristache, Anatoli Juditsky, Jörg Polzehl, and Vladimir Spokoiny. Structure adaptive approach for dimension reduction. *Annals of Statistics*, pages 1537–1566, 2001.

Leon Isserlis. On a formula for the product-moment coefficient of any order of a normal frequency distribution in any number of variables. *Biometrika*, 12 (1/2):134–139, 1918.

Arthur Jacot, Franck Gabriel, and Clément Hongler. Neural tangent kernel: Convergence and generalization in neural networks. *Advances in neural information processing systems*, 31, 2018.

Thorsten Joachims. Text categorization with support vector machines: Learning with many relevant features. In *European conference on machine learning*, pages 137–142. Springer, 1998.

Bobak Kiani, Jason Wang, and Melanie Weber. Hardness of learning neural networks under the manifold hypothesis. *Advances in Neural Information Processing Systems*, 37:5661–5696, 2024.

Samson Koelle, Hanyu Zhang, Marina Meilă, and Yu-Chia Chen. Manifold coordinates with physical meaning. *Journal of Machine Learning Research*, 23, 2022.

Alex Kokot and Alex Luedtke. Coreset selection for the sinkhorn divergence and generic smooth divergences. *arXiv preprint arXiv:2504.20194*, 2025.

Alex Kokot, Octavian-Vlad Murad, and Marina Meila. The noisy laplacian: a threshold phenomenon for non-linear dimension reduction. In *Forty-second International Conference on Machine Learning*, 2025.

Risi Kondor and Tony Jebara. A kernel between sets of vectors. In *Proceedings of the 20th international conference on machine learning (ICML-03)*, pages 361–368, 2003.

Jason D Lee, Kazusato Oko, Taiji Suzuki, and Denny Wu. Neural network learns low-dimensional polynomials with sgd near the information-theoretic limit. *Advances in Neural Information Processing Systems*, 37:58716–58756, 2024.

Hao Liu, Minshuo Chen, Tuo Zhao, and Wenjing Liao. Besov function approximation and binary classification on low-dimensional manifolds using convolutional residual networks. In *International Conference on Machine Learning*, pages 6770–6780. PMLR, 2021.

David G Lowe. Object recognition from local scale-invariant features. In *Proceedings of the seventh IEEE international conference on computer vision*, volume 2, pages 1150–1157. Ieee, 1999.

Wenjun Mei and Francesco Bullo. Lasalle invariance principle for discrete-time dynamical systems: A concise and self-contained tutorial. *arXiv preprint arXiv:1710.03710*, 2017.

Konstantin Mischaikow, Hal Smith, and Horst R Thieme. Asymptotically autonomous semiflows: chain recurrence and lyapunov functions. *Transactions of the American Mathematical Society*, 347 (5):1669–1685, 1995.

Alireza Mousavi-Hosseini, Sejun Park, Manuela Girotti, Ioannis Mitliagkas, and Murat A Erdogdu. Neural networks efficiently learn low-dimensional representations with sgd. *arXiv preprint arXiv:2209.14863*, 2022.

Sayan Mukherjee, Qiang Wu, and Ding-Xuan Zhou. Learning gradients on manifolds. 2010.

Francesca Odone, Annalisa Barla, and Alessandro Verri. Building kernels from binary strings for image matching. *IEEE Transactions on Image Processing*, 14(2): 169–180, 2005.

Michael Osborne. *Bayesian Gaussian processes for sequential prediction, optimisation and quadrature*. PhD thesis, Oxford University, UK, 2010.

Adityanarayanan Radhakrishnan, Daniel Beaglehole, Parthe Pandit, and Mikhail Belkin. Mechanism of feature learning in deep fully connected networks and kernel machines that recursively learn features. *arXiv preprint arXiv:2212.13881*, 2022.

Adityanarayanan Radhakrishnan, Mikhail Belkin, and Dmitriy Drusvyatskiy. Linear recursive feature machines provably recover low-rank matrices. *Proceedings of the National Academy of Sciences*, 122(13): e2411325122, 2025.

BLS Prakasa Rao. *Nonparametric functional estimation*. Academic press, 2014.

Alexander M Samarov. Exploring regression structure using nonparametric functional estimation. *Journal of the American Statistical Association*, 88(423):836–847, 1993.

Cordelia Schmid and Roger Mohr. Local grayvalue invariants for image retrieval. *IEEE transactions on pattern analysis and machine intelligence*, 19(5): 530–535, 1997.

Bernhard Schölkopf, Patrice Simard, Alex Smola, and Vladimir Vapnik. Prior knowledge in support vector

kernels. *Advances in neural information processing systems*, 10, 1997.

Erwan Scornet. Random forests and kernel methods. *IEEE Transactions on Information Theory*, 62(3):1485–1500, 2016.

Hiroyuki Takeda, Sina Farsiu, and Peyman Milanfar. Kernel regression for image processing and reconstruction. *IEEE Transactions on image processing*, 16(2):349–366, 2007.

Hiroyuki Takeda, Sina Farsiu, and Peyman Milanfar. Deblurring using regularized locally adaptive kernel regression. *IEEE transactions on image processing*, 17(4):550–563, 2008.

Anthony C Thompson. On certain contraction mappings in a partially ordered vector space. *Proceedings of the American Mathematical Society*, 14(3):438–443, 1963.

Carlo Tomasi and Roberto Manduchi. Bilateral filtering for gray and color images. In *Sixth international conference on computer vision (IEEE Cat. No. 98CH36271)*, pages 839–846. IEEE, 1998.

Shubhendu Trivedi, Jialei Wang, Samory Kpotufe, and Gregory Shakhnarovich. A consistent estimator of the expected gradient outerproduct. In *UAI*, pages 819–828, 2014.

Alexandre B. Tsybakov. *Nonparametric estimators*, pages 1–76. Springer New York, New York, NY, 2009. ISBN 978-0-387-79052-7. doi: 10.1007/978-0-387-79052-7_1. URL https://doi.org/10.1007/978-0-387-79052-7_1.

S Vichy N Vishwanathan, Nicol N Schraudolph, Risi Kondor, and Karsten M Borgwardt. Graph kernels. *The Journal of Machine Learning Research*, 11:1201–1242, 2010.

Martin J Wainwright. *High-dimensional statistics: A non-asymptotic viewpoint*, volume 48. Cambridge university press, 2019.

Wallraven, Caputo, and Graf. Recognition with local features: the kernel recipe. In *Proceedings Ninth IEEE International Conference on Computer Vision*, pages 257–264. IEEE, 2003.

Qiang Wu, Justin Guinney, Mauro Maggioni, and Sayan Mukherjee. Learning gradients: predictive models that infer geometry and statistical dependence. *The Journal of Machine Learning Research*, 11:2175–2198, 2010.

Yingcun Xia, Howell Tong, Wai Keung Li, and Li-Xing Zhu. An adaptive estimation of dimension reduction space. *Journal of the Royal Statistical Society Series B: Statistical Methodology*, 64(3):363–410, 2002.

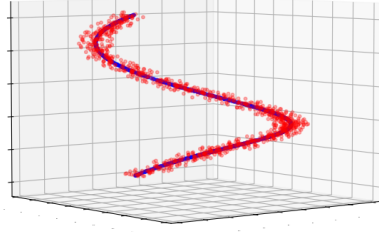
Gan Yuan, Mingyue Xu, Samory Kpotufe, and Daniel Hsu. Efficient estimation of the central mean subspace via smoothed gradient outer products. *arXiv preprint arXiv:2312.15469*, 2023.

Libin Zhu, Damek Davis, Dmitriy Drusvyatskiy, and Maryam Fazel. Iteratively reweighted kernel machines efficiently learn sparse functions. *arXiv preprint arXiv:2505.08277*, 2025.

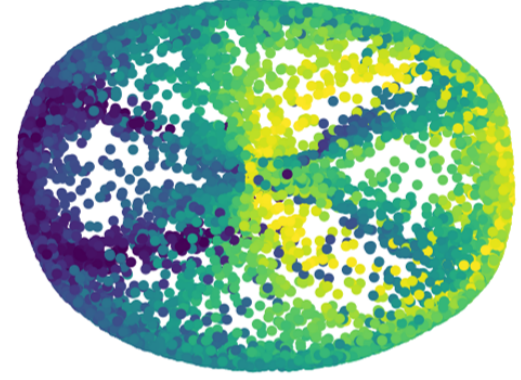
Local EGOP for Continuous Index Learning: Supplementary Material

A Experiment Details

The simulations were run on a machine of Intel® Xeon® processors with 48 CPU cores, and 50GB of RAM.



(a) 3-dimensional Helical data.



(b) Coordinates of Malonaldehyde embedded into 2 dimensions via Diffusion Maps [Coifman and Lafon, 2006] and colored by the backbone angles τ_1 .

A.1 General Set-up

In our synthetic experiments, to generate labeled data we randomly generated a homogeneous cubic polynomial

$$f(x) = \sum_{|\alpha| \leq 3} c_\alpha x^\alpha,$$

where $c_\alpha \sim \text{Uniform}[-3, 3]$. The resulting function f is then evaluated at the unperturbed datapoints before the features X were contaminated with noise orthogonal to the underlying manifold \mathcal{M} . The coefficients c_α are randomly sampled across each replicate of the experiments. We generically apply the below hyperparameters to the Local EGOP Learning algorithm in each example.

- number of EGOP iterations $T_{\text{test}} = 150$,
- Monte Carlo sample size $m = 300$,
- Bandwidth decay $t_i = (1 + i)^{-1.2}$,
- Initialization scale $\alpha = 0.2$
- Exclusion radius $\varepsilon = 1.6$

A.2 Two-layer Neural Network

We train fully connected NNs with both ReLU and GELU activations. All first layers use Kaiming initialization, and output layers are initialized at variance $1/\sqrt{m}$ where m is hidden width. All networks are trained with Adam.

For moderate-scale neural models, we conduct a grid search over hyperparameters. Widths are selected from 128, 256, 512, 1024, 2048, 4096, 8192, learning rates are selected from $10^{-3}, 3 \times 10^{-3}$, weight decay from 0, $10^{-5}, 10^{-4}$, and batch size from 16, 32, 64. The default Adam momentum parameters are used. Early stopping is applied with patience 200 and improvement tolerance 10^{-4} monitored on a validation split. In each experiment, only the optimal test error of these methods is aggregated into the “Small Tuned NN” plot.

We train overparameterized two-layer models with width 100,000, Adam with learning rate 0.003, batch size 64, and fixed weight decay 10^{-4} , applying early stopping with patience 300 and improvement tolerance 10^{-4} .

We also consider SIL models $f(x) = g(\beta^\top x)$, g a two-layer NN, with width 256 and GELU activations, β is normalized at each iteration.

A.3 Feature Learning

To qualitatively compare the local weighting behavior of EGOP with that of a learned neural embedding, we constructed a unified visualization pipeline producing animated opacity maps over a shared dataset. Both models were applied to the same two-dimensional manifold samples, with visualization frames showing how point-wise influence weights evolve during training or iteration.

Setup. We generated $n = 50,000$ samples on a spherical cap in \mathbb{R}^2 , restricted to an angular width of 25° . Each point x_i was scaled radially by a random factor $r_i \sim \text{Uniform}[r, R]$, with $r = 0.6$ and $R = 1.8$, and colored by the output of a random cubic polynomial $f(x)$. Additive Gaussian noise with standard deviation 0.05 was applied to the responses. The cap’s pole $x_0 = (1, 0)^\top$ was used as a fixed reference point for visualization of weight evolution.

We trained an `FTTransformer` regression model [Gorishniy et al., 2021] on this dataset using the `rtdl` and `zero` frameworks. The network was trained for 40 epochs with a batch size of 1024 and learning rate 2×10^{-3} . After every 50 training steps, we computed an embedding-based influence profile analogous to EGOP weights:

$$w_i = \frac{\exp(-\|z_i - z_0\|^2/\tau)}{\sum_j \exp(-\|z_j - z_0\|^2/\tau)},$$

where z_i denotes the learned feature representation of x_i , z_0 is the embedding of the reference point, and $\tau = 8.0$ is a temperature parameter controlling decay. These weights were rendered with the same opacity scheme as EGOP to enable direct visual comparison.

B Proofs

In our theory, we focus on the kernel $k = \exp(-\|x\|^2)$, as this allows for a direct correspondence to the risk distribution μ and its integration operators. We discuss general kernels in Appendix B.1.4.

B.1 Bias Control via EGOP

B.1.1 Bias Bound

To derive the upper bound from Lemma 1, we argue in stages. We first decompose the kernel smoother into two parts. The first is given by a pure Gaussian convolution and a density dependent covariance relating f and p . Both terms can readily be controlled via the EGOP-form, leading to our bound.

Define $\mu_M := N(x^*, M^{-1})$, $\mathbb{E}_M[\cdot] := \mathbb{E}_{\mu_M}[\cdot]$, Cov_M , Var_M similarly.

Lemma 6 (Basic Decomposition).

$$P_M f = \mathbb{E}_M f + \frac{\text{Cov}_M[f, p]}{\mathbb{E}_M p} =: G_M f + A_M f$$

Proof. We can simply compute

$$\begin{aligned} P_M f &= \frac{\mathbb{E}_M[fp]}{\mathbb{E}_M[p]} = \frac{\mathbb{E}_M[f]\mathbb{E}_M[p]}{\mathbb{E}_M[p]} + \frac{\text{Cov}_M[f,p]}{\mathbb{E}_M[p]} \\ &= \mathbb{E}_M[f] + \frac{\text{Cov}_M[f,p]}{\mathbb{E}_M[p]} =: \mathbb{E}_M[f] + A_M f. \end{aligned}$$

□

Lemma 7 (Gaussian Poincaré).

$$\int (\mathbb{E}_M[f] - f)^2 d\mu_M \leq W(\mu_M)$$

Proof. This is simply the Gaussian Poincaré inequality, see for instance Bakry et al. [2013][Proposition 4.1.1]. □

Lemma 8 (Poincaré \times p variance).

$$(A_M f)^2 \leq W(\mu_M) \frac{\text{Var}_M(p)}{\mathbb{E}_M[p]^2}$$

Proof.

$$A_M f^2 = \frac{\text{Cov}_M[f,p]^2}{\mathbb{E}_M[p]^2} \leq \frac{\text{Var}_M(f) \text{Var}_M(p)}{\mathbb{E}_M[p]^2} \leq W(\mu_M) \frac{\text{Var}_M(p)}{\mathbb{E}_M[p]^2},$$

applying the Gaussian Poincaré inequality Bakry et al. [2013][Proposition 4.1.1] for the last line. □

Proof of Lemma 1. We can apply Lemmas 7 and 8 immediately to yield

$$\int (P_M - f)^2 d\mu_M = \int (\mathbb{E}_M[f] - f + A_M f)^2 d\mu_M = \int (\mathbb{E}_M[f] - f)^2 d\mu_M + A_M f^2 \leq \left(1 + \frac{\text{Var}_M(p)}{\mathbb{E}_M[p]^2}\right) W(\mu_M).$$

Note that the density dependent factor $\frac{\text{Var}_M(p)}{\mathbb{E}_M[p]^2}$ is bounded by the continuity of p and the capped covariance assumptions. □

B.1.2 Variance Bound

We operate by a typical Nadaraya-Watson style argument. Our first steps are to show that the denominator of our estimator is very concentrated, allowing us to treat it as a constant up to a negligible residual. Let $\gamma_M \propto \det(M)^{1/2}$ by the normalization factor of μ_M . Define

$$\hat{C}'_M := \gamma_M \hat{C}_M := \gamma_M \frac{1}{n} \sum_{i=1}^n \exp(-(X_i - x^*)^T M(X_i - x^*)).$$

Lemma 9 (Denominator Concentration).

$$\mathbb{P}(|\hat{C}'_M - \mathbb{E}_M(p)| \leq \mathbb{E}_M(p)/2) \leq 2 \exp\left(-\frac{n\mathbb{E}_M(p)}{10\gamma_M}\right)$$

Proof. We prove this by applying Bernstein's inequality. First, observe $\mathbb{E}[\hat{C}_M] = G_M(p)$. Next, $\exp(-v^T M v) \in (0, 1]$ for any v , hence $\hat{C}'_M = \frac{\gamma_M}{n} \sum_{i=1}^n \exp(-(X_i - x)^T M(X_i - x))$ is the sample mean of iid bounded random variables in $(0, \gamma_M]$. Further, we can compute

$$\begin{aligned} \text{Var}[\gamma_M \exp(-(X_i - x)^T M(X_i - x))] &\leq \gamma_M \mathbb{E}[\gamma_M \exp(-(X_i - x)^T M(X_i - x))^2] \\ &\leq \gamma_M \mathbb{E}[\exp(-(X_i - x)^T M(X_i - x))] = \gamma_M G_M(p). \end{aligned}$$

Hence,

$$\begin{aligned}\mathbb{P}(|\hat{C}'_M - G_M(p)| \leq -G_M(p)/2) &\leq 2 \exp \left(-\frac{nG_M(p)^2}{8 \text{Var}(\gamma_M \exp(-(X_i - x)^T M(X_i - x))) + \frac{4}{3} \gamma_M G_M(p)^2} \right) \\ &\leq 2 \exp \left(-\frac{nG_M(p)^2}{8\gamma_M G_M(p) + \frac{4}{3} \gamma_M G_M(p)} \right) \leq 2 \exp \left(-\frac{nG_M(p)}{10\gamma_M} \right).\end{aligned}$$

□

Lemma 10 (Full Variance Expression). *Assume that the noise ε_i have finite fourth moments. Then, there exists a constant $C > 0$ such that*

$$\begin{aligned}\mathbb{E}[(\hat{P}_M(f) - P_M(f))^2] &\leq 2 \frac{\mathbb{E}[\gamma_M^2 \exp(-(X_i - x)^T M(X_i - x))^2 \{Y_i - P_M(f)\}^2]}{nG_M(p)^2} \\ &\quad + 2 \frac{\mathbb{E}[\{\gamma_M \exp(-(X_i - x)^T M(X_i - x)) Y_i\}^2]}{nG_M(p)^2} + C \exp \left(-\frac{nG_M(p)}{10\gamma_M} \right)\end{aligned}$$

Proof. Let E be the event $|\hat{C}_M - G_M(p)| \leq G_M(p)/2$. We compute

$$\begin{aligned}\hat{P}_M(f) - P_M(f) &= \frac{\frac{1}{n} \sum_{i=1}^n \gamma_M \exp(-(X_i - x^*)^T M(X_i - x)) Y_i}{\hat{C}'_M} - \frac{G_M(fp)}{G_M(p)} \\ &= \frac{\frac{1}{n} \sum_{i=1}^n [\gamma_M \exp(-(X_i - x^*)^T M(X_i - x^*)) \{Y_i - P_M(f)\}]}{G_M(p)} \mathbf{1}_E \\ &\quad + \frac{G_M(p) - \hat{C}'_M}{G_M(p) \hat{C}'_M} \frac{1}{n} \sum_{i=1}^n [\gamma_M \exp(-(X_i - x^*)^T M(X_i - x^*)) Y_i] \mathbf{1}_E \\ &\quad + \left\{ \frac{\frac{1}{n} \sum_{i=1}^n \gamma_M \exp(-(X_i - x^*)^T M(X_i - x^*)) Y_i}{\hat{C}'_M} - \frac{G_M(fp)}{G_M(p)} \right\} \mathbf{1}_{E^c}.\end{aligned}$$

Hence,

$$\begin{aligned}\mathbb{E}[(\hat{P}_M(f) - P_M(f))^2] &\leq 2 \frac{\mathbb{E}[\gamma_M^2 \exp(-(X_i - x^*)^T M(X_i - x^*))^2 \{Y_i - P_M(f)\}^2]}{nP_M(p)^2} \\ &\quad + 2\mathbb{E} \left[\left\{ \frac{G_M(p) - \hat{C}'_M}{G_M(p) \hat{C}'_M} \frac{1}{n} \sum_{i=1}^n [\gamma_M \exp(-(X_i - x^*)^T M(X_i - x^*)) Y_i] \right\}^2 \mathbf{1}_E \right] \\ &\quad + 2\mathbb{E} \left[\left\{ \hat{P}_M(f) - P_M(f) \right\}^2 \mathbf{1}_{E^c} \right].\end{aligned}$$

The first term is as desired. Next, by definition of the event, we have

$$\mathbb{E} \left[\left\{ \frac{G_M(p) - \hat{C}'_M}{G_M(p) \hat{C}'_M} \frac{1}{n} \sum_{i=1}^n [\gamma_M \exp(-(X_i - x^*)^T M(X_i - x^*)) Y_i] \right\}^2 \mathbf{1}_E \right] \leq \frac{\mathbb{E}[\{\gamma_M \exp(-(X_i - x^*)^T M(X_i - x^*)) Y_i\}^2]}{nG_M(p)^2}.$$

For the remaining term, observe that

$$\hat{P}_M(f) = \sum_{i=1}^n w_i Y_i$$

where w_i are a convex combination. Hence,

$$\mathbb{E} \left[\left\{ \hat{P}_M(f) - P_M(f) \right\}^2 \mathbf{1}_{E^c} \right] \leq \sqrt{\mathbb{E} \left[\left\{ 2\hat{P}_M(f)^2 + 2P_M(f)^2 \right\}^2 \right]} \mathbb{P}[E^c] \leq C \exp \left(-\frac{nG_M(p)}{10\gamma_M} \right),$$

by Lemma 9 and the hypothesis on the moments of ε_i and the boundedness of f . □

With this out of the way, we bound the two remaining expectations.

Lemma 11 (Normalization Constant). *There exists a constant $C > 0$ such that*

$$\begin{aligned}\mathbb{E}[\gamma_M^2 \exp(-((X_i - x^*)^T M(X_i - x^*))^2 \{Y_i - P_M(f)\}^2] &\leq C \gamma_M G_{2M}(p), \\ \mathbb{E}[\{\gamma_M \exp(-((X_i - x^*)^T M(X_i - x^*)) Y_i\}^2] &\leq C \gamma_M G_{2M}(p).\end{aligned}$$

Proof. Notice that $\gamma_M / \gamma_{4M} = C$ for some constant. Let $\varepsilon \sim \rho$. Focusing on the first expression,

$$\begin{aligned}\mathbb{E}[\gamma_M^2 \exp(-((X_i - x^*)^T M(X_i - x^*))^2 \{Y_i - P_M(f)\}^2] &= C \gamma_M \int \gamma_{4M} \exp(-(z - x)^T [2M](z - x)) p(y)(f(y) + \varepsilon - P_M(f))^2 dz d\rho(\varepsilon) \\ &= C \gamma_M \mathbb{E}_{2M}[p(x + Z) \mathbb{E}_\rho[(f(x + Z) + \mathcal{E} - P_M(f)(x))^2]] \leq C' \gamma_M G_{2M}(p)(x),\end{aligned}$$

using bounded moments and bounded f assumptions. Similarly,

$$\mathbb{E}[\{\gamma_M \exp(-((X_i - x^*)^T M(X_i - x^*)) Y_i\}^2] = C \gamma_M \mathbb{E}_{2M, \rho}[p(Z)[f(Z) + \mathcal{E}]^2] = C \gamma_M G_{2M}(p).$$

□

Combining these yields the desired variance bound multiplied by density dependent factors.

Proof of Lemma 2. By Lemmas 10 and 11, there exists a constant $C > 0$ such that

$$\mathbb{E}[(\hat{P}_M(f) - P_M(f))^2] \leq C \frac{\gamma_M}{n} \left(\frac{G_{2M}(p)}{G_M(p)^2} \right) + C \exp\left(-\frac{n}{\gamma_M} \left(\frac{G_M(p)}{10} \right)\right) = O\left(\frac{\sqrt{\det M}}{n}\right).$$

□

B.1.3 MSE

We compile the results from the previous section to provide guarantees for the MSE and MISE against Gaussians.

Proof of Theorem 1. Compiling Lemmas 1 and 2,

$$\begin{aligned}\mathbb{E}_M[(\hat{P}_M(f) - f)^2] &\leq C \frac{\sqrt{\det M}}{n} \left(\frac{G_{2M}(p)}{G_M(p)^2} \right) + C \exp\left(-\frac{n}{\sqrt{\det M}} \left(\frac{G_M(p)}{10} \right)\right) + C \left(1 + \frac{\text{Var}_{M_t}(p(Z))}{G_{M_t}(p)^2} \right) W(\mu_M) \\ &= O\left(\frac{\sqrt{\det M}}{n} + W(\mu_t)\right).\end{aligned}$$

□

B.1.4 General Kernels

In this section, we discuss which of results above are applicable to kernels of the form $k(M^{1/2}x)$. We start with the following Poincaré inequality. Let $\mu_{k,M}$ denote the probability distribution with density $\propto k(M^{1/2}[x - x^*])$.

Lemma 12 (Kernel Poincaré). *The measure $\mu_{k,M}$ has covariance proportionate to M^{-1} . If $\mu_{k,I}$ satisfies a Poincaré inequality with constant $1/C_I$, then*

$$\text{Var}_{\mu_{k,M}}(f) \leq \frac{1}{C_I} \int \nabla f^T M^{-1} \nabla f d\mu_{k,M}.$$

Proof. For convenience, we translate $x^* = 0$ without loss of generality. For the first claim, notice that when $M = I$, the density is symmetric about the origin, hence the covariance is proportionate to the identity. Thus the claim follows as $\mu_{k,M}$ is the pushforward of $\mu_{k,I}$ by $M^{-1/2}$.

Further,

$$\text{Var}_{\mu_{k,M}}(f) = \frac{1}{\sqrt{\det M}} \text{Var}_{\mu_{k,I}}(f \circ M^{-1/2}) \leq \frac{1}{C_I} \int \frac{1}{\sqrt{\det M}} \|\nabla f(M^{-1/2}y)\|^2 d\mu_{k,I}(y).$$

An application of the chain rule gives that

$$\nabla_y f(M^{-1/2}y) = M^{-1/2} \nabla f(M^{-1/2}y).$$

Substituting this into the bound above gives

$$\text{Var}_{\mu_{k,M}}(f) \leq \frac{1}{C_I} \int \frac{1}{\sqrt{\det M}} \|M^{-1/2} \nabla f(M^{-1/2}y)\|^2 \mu_{k,I}(y).$$

Changing variable back to $\mu_{k,M}$ yields the desired result. \square

With this in hand, the following is immediate for \hat{P}_M with k generic. The claim for the covariance similarly follows by change of variables, after observing that $\mu_{k,I}$ is rotation invariant, and therefore has isotropic covariance.

Corollary 2 (Kernel MSE). *Take k to be nonnegative, and satisfying a Poincaré inequality for isotropic covariance. Assume that f is bounded and ε_i has finite fourth moments. Then there exists an absolute constant C such that*

$$\begin{aligned} \mathbb{E} \left[\int (\hat{P}_M(f) - f)^2 d\mu_{k,M} \right] &\leq \\ C \frac{\sqrt{\det M}}{n} \left(\frac{\mathbb{E}_{\mu_{k^2,2M}}[p]}{\mathbb{E}_{\mu_{k,2M}}[p]^2} \right) + C \exp \left(-\frac{n}{\sqrt{\det M}} \left(\frac{\mathbb{E}_{\mu_{k,2M}}[p]}{10} \right) \right) + C \left(1 + \frac{\text{Var}_{\mu_{k,M}}(p)}{\mathbb{E}_{\mu_{k,M}}[p]^2} \right) W(\mu_{k,M}). \end{aligned}$$

B.2 Recursive Kernel Learning as Variance Minimization

The proof of Proposition 1 is clear from the main text, but we fill in the missing details here.

Proof of Proposition 1. The only thing left to clarify is the identity

$$tA^{-1}/D = \text{argmax}_{X \succeq 0, \text{tr}(AX) \leq t} \log \det X.$$

Note that $\log \det X$ is strictly convex, and KKT conditions yield that the minimum is a solution to the Lagrangian system of equations. Evaluating, we have

$$\mathcal{L}(X, \lambda) = \log \det X - \lambda(\text{tr}(AX) - t) \implies \nabla_X \mathcal{L} = X^{-1} - \lambda A = 0.$$

Hence the optimum is proportionate to A^{-1} , and evaluating the constraint yields the result. \square

B.3 Guarantees

To derive the learning rate for the Local EGOP Learning algorithm, we mostly operate at the level of matrices, studying the recurrence from Equation 7. To supplement this in the noisy manifold setting, we rely on critical geometric relations verified in Appendix B.3.2.

B.3.1 Sample Trimming

A practical concern when implementing the Local EGOP Learning algorithm is that two points $p, p' \in \mathcal{M}$ may be such that $p - p' \in \mathcal{N}_p$, but $f(p) \neq f(p')$. Such a function can still be continuous index as the line segment between these points goes beyond the reach of the manifold, and thus outside the data sampling region. A simple fix is to exclude data points outside of a fixed isotropic radius of the point of interest x^* , thus trimming the population distribution P . The resulting EGOP matrix will then be defined with respect to an extension outside this domain. We adopt such an extension so that Lemma 17, and the secondary conclusions of Lemma 5, that there is an affine space where the gradient is constant and the Hessian is degenerate, hold globally. Alternatively, one can broach this by taking the covariance cap to 0 at a logarithmic rate, reducing the sampling weight of the non-local region at the expense of a small variance inflation. For simplicity, we adopt the former assumptions.

B.3.2 Supporting Arguments for Lemma 4

We try to keep our proofs as elementary as possible. We start with basic properties of our function of interest f .

Lemma 13 (Derivatives). *Suppose that $f = f \circ \pi$. Then $\nabla f(x) \in \mathcal{T}_x$ and for any $u, v \in \mathcal{N}_x$, $u^T \nabla^2 f(x)v = 0$.*

Proof. Let $u, v \in \mathcal{N}_x$ be arbitrary. Then,

$$\nabla f(x)^T v = \lim_{t \rightarrow 0} [f(x + tv) - f(x)]/t = \lim_{t \rightarrow 0} [f(\pi[x + tv]) - f(\pi[x])]/t = \lim_{t \rightarrow 0} [f(\pi[x]) - f(\pi[x])]/t = 0,$$

as for small t orthogonal perturbations do not change the nearest point on \mathcal{M} . As this holds for generic v the first claim follows. To simplify notation, define $\partial_\eta h(x) := \lim_{t \rightarrow 0} [h(x + t\eta) - h(x)]/t$. We can thus compute

$$u^T \nabla^2 f(x)v = \partial_u (\nabla f^T v)(x) = 0$$

as $\nabla f^T v$ is identically 0 along the path $x + tv$, $t \in [0, \delta]$ for δ small enough. That is, as ∇f remains tangent along this path, as verified above, it is always orthogonal to v . \square

In the interest of further studying the structure of ∇f we verify the following fundamental Geometric facts. We denote by π_V the projection onto the vector space V . Denote by $d(\cdot, \cdot)$ the geodesic distance on \mathcal{M} . Let $\kappa = \sup_{p \in \mathcal{M}, \|v\|=1} \|S_v(p)\|$, S the Weingarten map of \mathcal{M} . This constant is automatically finite as \mathcal{M} has nontrivial reach.

Lemma 14 (Orthogonal Curvature). *There exists a universal constant C such that, for any $p, p^* \in \mathcal{M}$,*

$$\|\pi_{\mathcal{N}_p} - \pi_{\mathcal{N}_{p^*}}\| \leq Cd(p, p^*).$$

Proof. Let γ_t , $t \in [0, d(p, p^*)]$ be a unit speed geodesic connecting p and p^* . We can compute

$$\|\pi_{\mathcal{N}_p} - \pi_{\mathcal{N}_{p^*}}\| = \left\| \int_0^1 \partial_t \pi_{\mathcal{N}_{\gamma_t}} dt \right\| \leq \int_0^{d(p, p^*)} \|\partial_t \pi_{\mathcal{N}_{\gamma_t}}\| dt.$$

Thus, if we can show a uniform bound for $\|\partial_t \pi_{\mathcal{N}_{\gamma_t}}\|$ then we are done.

Let v_1, \dots, v_{D-d} be an orthonormal basis of \mathcal{N}_{p^*} , and form the orthonormal moving frame $v_1(t), \dots, v_{D-d}(t)$ along γ_t by parallel translation. Let

$$V(t) := [v_1(t) \quad \dots \quad v_{D-d}(t)].$$

By construction, $\pi_{\mathcal{N}_{\gamma_t}} = V(t)V(t)^T$, $V(t)$ is orthogonal for all t . Differentiating,

$$\|\partial_t \pi_{\mathcal{N}_{\gamma_t}}\| = \|V'(t)V(t)^T + V(t)V'(t)^T\| \leq 2\|V'(t)\|\|V(t)\| = 2\|V'(t)\|.$$

This reduces the problem to uniformly bounding $\|V'(t)\|$. The key relations to prove this are

$$V'(t) = [v'_1(t) \quad \dots \quad v'_{D-d}(t)], \quad v'_i(t) = -S_{v_i(t)}(\gamma_t)\gamma'_t.$$

The first identity is definitional, the second can be found in Do Carmo [2016]. For $\|u\| = 1$, we have

$$\|V'(t)u\| = \left\| \sum_{i=1}^{D-d} u_i v'_i(t) \right\| = \left\| -S_{\sum_i u_i v_i(t)}(\gamma_t)\gamma'_t \right\| \leq \|S_{\sum_i u_i v_i(t)}(\gamma_t)\gamma'_t\| \leq \kappa,$$

as $\|\sum_i u_i v_i(t)\| \leq \sum_i u_i^2 = 1$, hence $\|V'(t)\| \leq \kappa$ holds uniformly. \square

Lemma 15 (Projection Normal). *For any $v \in \mathcal{N}_{\pi[x]}$, $D\pi_x v = 0$.*

Proof. As computed previously,

$$D\pi_x v = \lim_{t \rightarrow 0} [\pi[x + tv] - \pi[x]]/t = 0.$$

\square

Lemma 16 (Orthogonal Control). *Fix x^* in the tubular neighborhood of \mathcal{M} . There exists $r > 0$ small enough such that, for $\|x - x^*\| \leq r$, there exists a constant $C > 0$ such that*

$$\|\pi_{\mathcal{N}_{x^*}} - \pi_{\mathcal{N}_x}\| \leq C\|\pi_{\mathcal{T}_{x^*}}[x^* - x]\|$$

Proof. By Lemma 14, it suffices to show that $d(\pi[x^*], \pi[x]) = O(\|\pi_{\mathcal{T}_{x^*}}[x^* - x]\|)$. By Garcia Trillo [2019], we have that $d(\pi[x^*], \pi[x]) = O(\|\pi[x^*] - \pi[x]\|)$, further reducing the problem. By our locality assumption, we can take convex combinations and remain within the tubular neighborhood, allowing us to decompose

$$\|\pi[x^*] - \pi[x]\| \leq \left\| \int_0^1 D\pi_{x^* + t(x-x^*)}(x - x^*) dt \right\| \leq \int_0^1 \|D\pi_{x^* + t(x-x^*)}(x - x^*)\| dt.$$

By Lemma 18,

$$\begin{aligned} \|D\pi_{x^* + t(x-x^*)}(x - x^*)\| &= \|D\pi_{x^* + t(x-x^*)}(\pi_{\mathcal{T}_{x^* + t(x-x^*)}}[x - x^*])\| \leq C\|\pi_{\mathcal{T}_{x^* + t(x-x^*)}}[x - x^*]\| \\ &\leq C\|\pi_{\mathcal{T}_{x^* + t(x-x^*)}} - \pi_{\mathcal{T}_{x^*}}\| \|x - x^*\| + C\|\pi_{\mathcal{T}_{x^*}}[x - x^*]\| \leq Cr\|\pi_{\mathcal{T}_{x^* + t(x-x^*)}} - \pi_{\mathcal{T}_{x^*}}\| + C\|\pi_{\mathcal{T}_{x^*}}[x - x^*]\|, \end{aligned}$$

as π is smooth, and we have restricted ourselves to a bounded domain. In other words,

$$\|\pi[x^*] - \pi[x]\| - Cr\|\pi_{\mathcal{T}_{x^* + t(x-x^*)}} - \pi_{\mathcal{T}_{x^*}}\| \leq C\|\pi_{\mathcal{T}_{x^*}}[x - x^*]\|,$$

hence, if we can show that

$$\|\pi_{\mathcal{T}_{x^* + t(x-x^*)}} - \pi_{\mathcal{T}_{x^*}}\| \leq C'\|\pi[x^*] - \pi[x]\|,$$

then for r small enough the desired inequality will be achieved. Notice that $\pi_{\mathcal{T}_x} = I - \pi_{\mathcal{N}_x}$, hence by Lemma 14

$$\|\pi_{\mathcal{T}_{x^* + t(x-x^*)}} - \pi_{\mathcal{T}_{x^*}}\| = \|\pi_{\mathcal{N}_{x^* + t(x-x^*)}} - \pi_{\mathcal{N}_{x^*}}\| \leq \tilde{C}d(\pi[x^*], \pi[x^* + t(x - x^*)]) \leq C'\|\pi[x^*] - \pi[x]\|,$$

completing the proof. \square

We apply this to study ∇f .

Lemma 17 (Gradient Rotation). *Restricting ourselves to a region small enough that Lemma 16 is valid, we have*

$$\|\pi_{\mathcal{N}_{x^*}} \nabla f(x)\| = O(\|\pi_{\mathcal{T}_{x^*}}[x^* - x]\|).$$

Proof. By Lemmas 13 and 16,

$$\|\pi_{\mathcal{N}_{x^*}} \nabla f(x)\| = \|[\pi_{\mathcal{N}_{x^*}} - \pi_{\mathcal{N}_x}] \nabla f(x)\| \leq C\|\pi_{\mathcal{N}_{x^*}} - \pi_{\mathcal{N}_x}\| \leq C'\|\pi_{\mathcal{T}_{x^*}}[x^* - x]\|.$$

\square

B.3.3 Supporting Arguments for Lemma 5

Lemma 18. *Let $x \in \mathcal{M}$ and $\eta \in \mathcal{N}_x$. Then $D\pi_{x+\eta} = (I - S_x(\eta))^{-1}\pi_{\mathcal{T}_x}$.*

Proof. Clearly, for any normal vector $v \in \mathcal{N}_x$, $D\pi_{x+\eta}v = 0$, as projection is invariant to normal displacement. Thus it suffices to verify the formula for any tangent vector. Our proof has two primary parts. First, we pass to normal coordinates, equating the tubular neighborhood about \mathcal{M} with the normal bundle, and compute the differential of the exponential map. From this parameterization, we can then analyze the projection via the chain rule.

Starting from the normal bundle $N\mathcal{M}$, for $(x, v) \in N_x\mathcal{M}$, the exponential map $E(x, v) = x + v$ is a diffeomorphism to the tube. Let $\gamma(t) = (u(t), \xi(t)) \in N\mathcal{M}$, $\gamma'(t) \in TN\mathcal{M}$. We compute $\xi'(0) = -S_x(v)u'(0) + \nabla_{u'(0)}^\perp \xi(0)$, hence

$$DE_{(x,v)}\gamma'(0) = u + [-S_x(v)u + \nabla_{u'(0)}^\perp \xi(0)] = (I - S_x(v))u + \nabla_{u'(0)}^\perp \xi(0).$$

Composing with the projection map, $\pi \circ E(x, v) = x$, hence

$$D\pi_{x+v}DE_{(x,v)}\gamma'(0) = u'(0) \iff D\pi_{x+v}\pi_{\mathcal{T}_x}[(I - S_x(v))u] = u'(0),$$

and inverting yields the claim, as $D\pi_{x+v}$ is a linear operator. \square

Proof of Lemma 5. The first claim follows immediately from Lemma 18 and the chain rule, indeed,

$$\nabla f(x + v) = \nabla g(\pi(x + v)) = (I - S_x(v))^{-1} \nabla g(x).$$

Let $u = (I - S_x(v))^{-1} \nabla g(x)$. Applying linearity of the shape operator, observe that $(I - S_x(v + \eta))u = (I - S_x(v))u - S_x(\eta)(u) = \nabla g(x) - S_x(\eta)u$. Hence, if $S_x(\eta)u = 0$ then $u = \nabla f(x + v + \eta)$. Thus, the second claim follows if we can show that there is a $D - 2d$ dimensional subspace Null that annihilates the solution vector u . For $w \in \mathcal{T}_x$,

$$\langle S_x(\eta)u, w \rangle = \langle \mathbb{I}(u, w), \eta \rangle$$

for \mathbb{I} the second fundamental form. This is a bilinear map, and the map defined by fixing the u argument, $\phi_u(w) := \mathbb{I}(u, w)$ is a linear map from $\mathcal{T}_x \rightarrow \mathcal{N}_x$, and thus has image no larger than d . Its complement $\phi_u(\mathcal{T}_x)^\perp$ has dimension at least $\dim(\mathcal{N}_x) - d = D - 2d$, as desired.

This proves the invariance of the gradient along a space of dimension at least $D - 2d$, which immediately implies $\nabla^2 f(x + v + \eta)z = \partial_z \nabla f(x + v) = 0$.

□

B.3.4 Taylor Expansion

We first provide the generic Taylor expansion, which we then go on to refine for the noisy manifold setting.

Proof of Lemma 3. We start by Taylor expanding the gradient. For a D tuple ξ , as $\partial_\xi \partial_i f = \partial_i \partial_\xi f$, for f sufficiently smooth we can express

$$\partial_i f(x) = \sum_{|\xi| \leq q} \frac{1}{q!} \partial_i [\partial_\xi f](x) \prod_{q_i \in \xi} x_i^{q_i} + O(\|x\|^{q+1}).$$

In particular, we have

$$\partial_i f(x) = \partial_i f(0) + \sum_j \partial_i \partial_j f(0) x_j + \frac{1}{2} \sum_{j,k} \partial_i \partial_j \partial_k f(0) x_j x_k + O(\|x\|^3).$$

Working at the level of the gradient, this yields

$$\nabla f(x) = \nabla f(0) + \nabla^2 f(0)x + T(x, x) + O(\|x\|^3)$$

where T is the bilinear for

$$[T[x, y]]_i = \frac{1}{2} \sum_{j,k} \partial_i \partial_j \partial_k f(0) x_j y_k.$$

We use the first three terms of this Taylor expansion as a starting point. Set $g := \nabla f(0)$, $H := \nabla^2 f(0)$.

The remainder of the Taylor expansion can be exactly expressed as

$$\tilde{R}(x) = \frac{1}{6} \int_0^1 (1-s)^2 \nabla^4 f(sx)[x, x, x] ds, \quad [\nabla^4 f(sx)[x, x, x]]_i := \sum_{j,k,\ell} \partial_i \partial_j \partial_k \partial_\ell f(sx) x_i x_j x_k.$$

Hence, under our uniform boundedness assumption, we have

$$\|T[x, x]\| \leq C\|x\|^2, \quad \|\tilde{R}(x)\| \leq C\|x\|^3$$

for some constant C . Throughout the argument, for convenience we will absorb constants into C if necessary. Hence,

$$\mathcal{L}(\mu) = \int \nabla f \nabla f^T d\mu = gg^T + H\Sigma H + gT(\Sigma)^T + T(\Sigma)g^T + R(\Sigma),$$

for

$$\begin{aligned} T(\Sigma)_i &:= \mathbb{E}_\mu[T(x, x)_i] = \frac{1}{2} \sum_{j,k} \partial_i \partial_j \partial_k f(0) \Sigma_{jk} \\ R(\Sigma) &:= \mathbb{E}_\mu[T[Z, Z]T[Z, Z]^T + HZ\tilde{R}(Z)^T + \tilde{R}(Z)(HZ)^T + \tilde{R}(Z)\tilde{R}(Z)^T]. \end{aligned}$$

That T is continuous and linear in Σ is immediate. For the remainder, we have

$$\begin{aligned}\|R(\Sigma)\| &\leq \mathbb{E}_\mu[\|T[Z, Z]T[Z, Z]^T\| + \|HZ\tilde{R}(Z)^T\| + \|\tilde{R}(Z)(HZ)^T\| + \|\tilde{R}(Z)\tilde{R}(Z)^T\|] \\ &\leq C\mathbb{E}[\|Z\|^4 + \|Z\|^6] \leq C\mathbb{E}_\mu[\text{tr}(\Sigma^2) + \text{tr}(\Sigma)^2]\end{aligned}$$

where we apply Isserlis's Theorem [1918] to relate moments of the norm to the covariance matrix, and our capped covariance assumption is used to compress all higher order terms to quadratic order. Our proof is completed upon observing

$$\text{tr}(\Sigma^2) = \|\Sigma\|_F^2, \quad \text{tr}(\Sigma)^2 = \left(\sum_i \lambda_i\right)^2 \leq D \sum_i \lambda_i^2 = D\|\Sigma\|_F^2,$$

and in finite dimensions the frobenius and operator norms are equivalent. \square

Proof of Lemma 4. That $\text{rank}(H) \leq 2d$ is immediate from Lemma 13. Indeed, the $\mathcal{N} \times \mathcal{N}$ block of H is completely 0, hence at most d rows and d columns of H in the $\mathcal{T} \oplus \mathcal{N}$ basis have nonzero entries. Let B_r be

We now apply Lemmas 13 and 17 to compute

$$\begin{aligned}\|\pi_{\mathcal{N}}\mathcal{L}(\mu)\pi_{\mathcal{N}}\| &= \left\| \int \pi_{\mathcal{N}}\nabla f \nabla f^T \pi_{\mathcal{N}} d\mu \right\| \leq \int \|\pi_{\mathcal{N}}\nabla f \nabla f^T \pi_{\mathcal{N}}\| d\mu = \int \|[\pi_{\mathcal{N}} - \pi_{\mathcal{N}_x}]\nabla f(x)\nabla f(x)^T[\pi_{\mathcal{N}} - \pi_{\mathcal{N}_x}]\| d\mu \\ &\leq C \int \|\pi_{\mathcal{N}} - \pi_{\mathcal{N}_x}\|^2 d\mu \leq C \int \|\pi_{\mathcal{T}}x\|^2 d\mu \leq C[\text{tr}([\pi_{\mathcal{T}}\Sigma\pi_{\mathcal{T}}]^2) + \text{tr}(\pi_{\mathcal{T}}\Sigma\pi_{\mathcal{T}})^2] \leq C\|\pi_{\mathcal{T}}\Sigma\pi_{\mathcal{T}}\|_F^2,\end{aligned}$$

where the final bounds from Isserlis's Theorem are similar to Lemma 3. Similarly,

$$\|\pi_{\mathcal{T}}\mathcal{L}(\mu)\pi_{\mathcal{N}}\| \leq \int \|\pi_{\mathcal{T}}\nabla f(x)\nabla f(x)^T[\pi_{\mathcal{N}} - \pi_{\mathcal{N}_x}]\| d\mu \leq C \int \|\pi_{\mathcal{T}}x\| d\mu \leq C \sqrt{\int \|\pi_{\mathcal{T}}x\|^2 d\mu} = C\|\pi_{\mathcal{T}}\Sigma\pi_{\mathcal{T}}\|_F.$$

As the operator and Frobenius norms are equivalent the bounds are as desired. \square

Proof of Corollary 1. The basic claim is immediate from Lemma 3, and that the terms stemming from higher order derivatives are uniformly bounded follows from the smoothness assumptions on f . Further, the nullspace of the Hessian and the 0 order expansion being the gradient $g = \nabla f(x^*)$ follow immediately from Lemma 5. \square

B.3.5 Matrix Recurrence

We begin our study of the recurrence in Equation 7 by introducing a reduced form. We analyze this scheme, and then apply it to Local EGOP Learning, leveraging the results of Appendix B.3.2. We divide our focus into two distinct settings, the first mirroring Equation 9 by introducing a constant shift, and the second mirroring Equation 8 a homogeneous equation.

Constant Shift

Let J be an involution, $J = J^T = J^{-1}$. We introduce the recurrence

$$B_{i+1} = t_{i+1}J(G + \beta B_i + (1 - \beta)B_{i-1} + E_i)^{-1}J$$

where E_i is an error term, $\beta \in (0, 1)$, $G \succ 0$, $B_0 = \alpha I$, $t_1 = \alpha^2$, $B_1 = t_1 J(G + B_0)^{-1}J$, $t_{i+1} = t_i r^2$, $r < 1$.

Lemma 19 (Perturbed Shift). *Suppose there exists a uniform constant C such that $\|E_i\| \leq C\alpha$ for all i . Then, for α small enough,*

$$\|B_{i+1}\| = \Theta(t_i).$$

Proof. That α must be small is not necessary, but this will be a typical setting and will help expedite the proof. Let $\alpha < 1$ be small enough that $\|B_i\| \leq \lambda_{\min}(G)/4$, $i = 1, 2$, and $C\alpha \leq \lambda_{\min}(G)/4$. We prove by strong induction that $\|B_{i+1}\| \leq t_{i+1} \frac{2}{\lambda_{\min}(G)}$. The base case is already proven, so we move on to the inductive step. We can simply compute

$$G + \beta B_i + (1 - \beta)B_{i-1} + E_i \succeq G/2.$$

As J is an orthogonal matrix, we have $\|B_{i+1}\| \leq 2t_{i+1}/\lambda_{\min}(G)$ and the claim follows.

With the decay of B_i being settled, it follows that $B_i = t_{i+1}JG^{-1}J + O(t_{i+1}^2 + \alpha)$, hence, normalizing by t_{i+1} , we have exact convergence to $JG^{-1}J$ in the noiseless setting. \square

Note that the geometric decay and many of the assumptions were not completely necessary for this proof, however we introduce them now as they will greatly facilitate the following arguments.

Homogeneous

We move on to the recurrence

$$A_{i+1} = t_{i+1}J(\beta A_i + (1 - \beta)A_{i-1} + E_i)^{-1}J$$

where E_i is an error term, J is an involution, $\beta \in (0, 1)$, $G \succ 0$, $B_0 = \alpha I$, $t_1 = \alpha^2$, $B_1 = t_1 J(G + B_0)^{-1}J$, $t_{i+1} = t_i r^2$, $r < 1$.

We start by reducing this iteration scheme to an autonomous equation.

Proposition 2 (Autonomous Recurrence). *Define $c(r, \beta) := \frac{1}{\beta/r + (1-\beta)/r^2}$ and let $X_i := A_i/\sqrt{c(r, \beta)t_i}$, $R_i := \sqrt{c(r, \beta)}E_i/\sqrt{t_{i+1}}$, and $\eta = \frac{\beta/r}{c(r, \beta)}$. Then X_i satisfies the autonomous recurrence*

$$X_{i+1} = J(\eta X_i + (1 - \eta)X_{i-1} + R_i)^{-1}J$$

Proof. We work this out by simple algebra. First, as an intermediate step, introduce $C_i := A_i/\sqrt{t_i}$, $R'_i := E_i/\sqrt{t_{i+1}}$. Then we can write

$$\begin{aligned} A_{i+1} = t_{i+1}J(\beta A_i + (1 - \beta)A_{i-1} + E_i)^{-1}J &\iff \frac{A_{i+1}}{\sqrt{t_{i+1}}} = J \left(\beta \frac{A_i}{\sqrt{t_{i+1}}} + (1 - \beta) \frac{A_{i-1}}{\sqrt{t_{i+1}}} + \frac{E_i}{\sqrt{t_{i+1}}} \right)^{-1} J \\ &\iff C_{i+1} = J([\beta/r]C_i + [(1 - \beta)/r^2]C_{i-1} + R'_i)^{-1}J \iff C_{i+1} = c(r, \beta)J(\eta C_i + (1 - \eta)C_{i-1} + R'_i c(r, \beta))^{-1}J \\ &\iff \frac{C_{i+1}}{\sqrt{c(r, \beta)}} = J \left(\eta \frac{C_i}{\sqrt{c(r, \beta)}} + (1 - \eta) \frac{C_{i-1}}{\sqrt{c(r, \beta)}} + R'_i \sqrt{c(r, \beta)} \right) J \iff X_{i+1} = J(\eta X_i + (1 - \eta)X_{i-1} + R_i)^{-1}J. \end{aligned}$$

\square

Thus to study A_i it suffices to study X_i , then multiply by the corresponding factors. Our analysis proceeds as follows. First, leveraging the Thompson metric [Thompson, 1963], we show that, for summable error R_i , the spectrum of X_i stays bounded away from 0 and ∞ . Then, utilizing this bound, we go on to show that $X_i \rightarrow I$ up to some error controlled by α . Define the Thompson metric,

$$d_T(A, B) := \log \max\{M(A/B), M(B/A)\}, \quad M(A/B) := \inf\{\gamma > 0 : A \preceq \gamma B\}.$$

Lemma 20 (Spectral Band). *Suppose that $\sum_i \|R_i\| \leq C\alpha$ and $\max\{d_T(X_0, I), d_T(X_1, I)\} = L_0$. Then, for α sufficiently small,*

$$[e^{-L_0} - O(\alpha)]I \preceq X_i \preceq [e^{L_0} + O(\alpha)]I$$

for all i .

Proof. Notice that

$$(1 - \xi_i)[\eta X_i + (1 - \eta)X_{i-1}] \preceq \eta X_i + (1 - \eta)X_{i-1} + R_i \preceq (1 + \xi_i)[\eta X_i + (1 - \eta)X_{i-1}]$$

for $\xi_k := \|[\eta X_i + (1 - \eta)X_{i-1}]^{-1/2} R_i [\eta X_i + (1 - \eta)X_{i-1}]^{-1/2}\|$. It follows that

$$d_T([\eta X_i + (1 - \eta)X_{i-1}] + R_i, [\eta X_i + (1 - \eta)X_{i-1}]) \leq \log \frac{1 + \xi_i}{1 - \xi_i}$$

Hence, if $e^{-L_i}I \preceq X_i, X_{i-1} \preceq e^{L_i}I$, it follows that $\xi_i \leq e^{L_i} \|R_i\|$ and

$$L_{i+1} \leq L_i + \log \frac{1 + \|R_i\|e^{L_i}}{1 - \|R_i\|e^{L_i}} \iff e^{-L_{i+1}} \geq e^{-L_i} \left(\frac{e^{-L_i} + \|R_i\|}{e^{-L_i} - \|R_i\|} \right) \implies e^{-L_{i+1}} \geq e^{-L_i} - 2\|R_i\|.$$

Thus,

$$e^{-L_i} \geq e^{-L_0} - 2 \sum_{i=1}^{\infty} \|R_i\| \geq e^{-L_0}/2$$

choosing α sufficiently small. \square

Lemma 21 (Non-Expansive). *Let X_i, X'_i be autonomous homogeneous recurrences of the Proposition 2 form, with common conjugation matrix J . Then*

$$d_T(X_{i+1}, X'_{i+1}) \leq \max\{d_T(X_i, X'_i), d_T(X_{i-1}, X'_{i-1})\} + O(\|R_i\| + \|R'_i\|)$$

Proof. Set $M_i = \eta X_i + (1 - \eta)X_{i-1}$, $M'_i = \eta X'_i + (1 - \eta)X'_{i-1}$. Using the invariance of the Thompson metric to conjugation by orthogonal matrices and inversion, we can compute

$$\begin{aligned} d_T(X_{i+1}, X'_{i+1}) &= d_T(\eta X_i + (1 - \eta)X_{i-1} + R_i, \eta X'_i + (1 - \eta)X'_{i-1} + R'_i) \\ &\leq d_T(M_i, M'_i) + d_T(M_i, M_i + R_i) + d_T(M'_i, M'_i + R'_i). \end{aligned}$$

Checking each term,

$$d_T(M_i, M'_i) \leq \max\{d_T(X_i, X'_i), d_T(X_{i-1}, X'_{i-1})\}$$

as averaging in the Thompson metric is non-expansive.

$$d_T(A, A + A) = \|\log A^{-1/2}(A + E)A^{-1/2}\| = \|\log(I + A^{-1/2}EA^{-1/2})\| = O(\|E\|)$$

for A with non-vanishing spectrum. Lemma 20 verifies that the sequences X_i, X'_i do not degenerate for α sufficiently small, thus showing the claim. \square

Lemma 22 (Definite Hessian). *Let $J = I$. Then for α sufficiently small, $X_i \rightarrow I$.*

Proof. Define $T(x, y) = ((\eta x + (1 - \eta)y)^{-1}, x)$, hence $T(X_i, X_{i-1}) = (X_{i+1}, X_i)$. Define

$$V(x, y) = \max\{d_T(x, I), d_T(y, I)\} = \max\{|\log \lambda_{\max}(x)|, |\log \lambda_{\max}(y)|, |\log \lambda_{\min}(x)|, |\log \lambda_{\min}(y)|\}.$$

Notice that

$$\min\{\lambda_{\min}(x), \lambda_{\min}(y)\} \leq \lambda_{\min}(\eta x + (1 - \eta)y)^{-1} \leq \lambda_{\max}(\eta x + (1 - \eta)y)^{-1} \leq \max\{\lambda_{\max}(x), \lambda_{\max}(y)\}$$

hence $V(T(X_i, X_{i-1})) \leq V(X_i, X_{i-1})$. Thus the noiseless recurrence is autonomous, and the discrete Lasalle invariance principle [Mei and Bullo, 2017, Theorem 2] yields the existence of a set E_c , $T(E_c) \subseteq E_c$ such that for all $(X, Y) \in E_c$, $V(E_c) = c$ and $\lim_{i \rightarrow \infty} \inf_{E \in E_c} \|(X_i, X_{i-1}) - E\| \rightarrow 0$. To verify that $X_i \rightarrow I$ in the noiseless case, it suffices to show $E_0 = \{(I, I)\}$ is the only invariant set with constant value function.

We argue by contradiction. Let E_c be such a limit set, $c > 0$. Take $(X_1, X_0) \in E_c$, and consider $(X_3, X_2) = T^2(X_1, X_0)$. By the condition on the value function V , either the largest eigenvalue of these matrices is e^c or the smallest is e^{-c} . Without loss of generality, assume that X_3 achieves the eigenvalue e^c .

For this to occur, it must be that both X_2, X_1 have eigenvalue e^{-c} with a common eigenvector v . As the sequence is rational in X_2, X_1 , v will be an eigenvector for all subsequent matrices X_i . Notice $\log \lambda_v(X_4) = -\log(\eta e^c + (1 - \eta)e^{-c}) \in (-c, c)$, hence $\sup_{i > 0} |\log \lambda_v(X_{3+i})| < c$, and this eigenspace can never again be extremal. Indeed, for $\lambda_v(X_{3+i}) = e^{\pm c}$, we require $\lambda_v(X_{2+i}) = \lambda_v(X_{1+i}) = e^{\mp c}$, thus any extremal eigenspace for $T^2(X_1, X_0)$ will decay upon further iterations, and non-extremal eigenspaces cannot become extremal. In particular, $V(T^k(X_1, X_0))$ must decrease as $k \rightarrow \infty$, contradicting that E_c is invariant with fixed value function $V(E) = c$ for all $E \in E_c$.

In the noisy setting, Lemma 20 verifies that the recurrence remains compact for α sufficiently small. Hence, we can apply [Mischaikow et al., 1995, Theorem 1.8] to verify that the perturbed recurrence converges to the same limit sets as the autonomous recurrence, i.e. I is the unique limit point. \square

Lemma 23 (Generic J). *Suppose that J has signature (k, j) . Then, for α sufficiently small, $X_i \rightarrow L \in \{X : (XJ)^2 = I\}$. Further, L has at most $2 \min\{k, j\}$ eigenvalues not equal to 1.*

Proof. We update the recurrence in Lemma 22 by J congruence. V is still monotone in the autonomous noiseless recurrence as J is orthogonal. We begin by investigating the structure of any invariant set E_c .

As in the previous proof, if we initialize with a pair in E_c , then for any $i \geq 2$, and all extremal eigenpairs (λ_ℓ, v_ℓ) , it must be that for both $j = i-1, i-2$, the matrices X_j have matching eigenpairs $(1/\lambda_\ell, Jv_\ell)$. Repeating this argument for X_{i+1} , for any extremal eigenpairs (ν_ℓ, u_ℓ) it follows that X_i, X_{i-1} have matching eigenpairs $(1/\nu_\ell, Ju_\ell)$. Combining this information, for each extremal eigenpair (ν_ℓ, u_ℓ) of X_{i+1} , $(1/\nu_\ell, Ju_\ell)$ must be an eigenpair of both X_i and X_{i-1} . As $(\lambda_\ell, v_\ell) = (1/\nu_\ell, Ju_\ell)$ is an extremal eigenpair of X_i , it must also be that (ν_ℓ, u_ℓ) is an eigenpair of X_{i-1} . Hence the matrix X_{i-1} has both $(1/\nu_\ell, Ju_\ell)$ and (ν_ℓ, u_ℓ) as extremal eigenpairs, and for them to pass forward in the recurrence they must be shared by X_{i-1} . Thus we see that for all $m \geq i$, $(1/\nu_\ell, Ju_\ell)$ and (ν_ℓ, u_ℓ) are fixed eigenvectors of X_m .

Thus we have proven that any limiting set in E_c has fixed, cyclical extremal eigenpairs. Suppose that X_i has κ such limiting maximal eigenvalues. Let $\text{Trunc}_\kappa(X)$ be the map that identifies X with the $(D-\kappa) \times (D-\kappa)$ matrix formed by removing the principal κ components. Thus, $\text{Trunc}_\kappa T(X_{i+1}, X_i) = T(\text{Trunc}_\kappa(X_i, X_{i-1})) + o(1)$, and the sequence $\text{Trunc}_\kappa(X_i, X_{i-1})$ is asymptotically autonomous and monotone in the value function V . Hence [Mischaikow et al., 1995, Theorem 1.8] yields that the truncated sequence has asymptotically cyclical extremal eigenvectors.

Inductively applying this argument verifies that $X_i \rightarrow L$ for a fixed matrix L in the noiseless case. By definition

$$L = \lim_{i \rightarrow \infty} X_{i+1} = \lim_{i \rightarrow \infty} J(\eta X_{i+1} + (1-\eta)X_i)^{-1}J = JL^{-1}J,$$

hence $L \in \{X : (LJ)^2 = I\}$. In the noisy setting, Lemma 20 verifies that the recurrence remains compact for α sufficiently small. Hence, we can apply [Mischaikow et al., 1995, Theorem 1.8] to verify that the perturbed recurrence converges to the same limit sets as the autonomous recurrence.

We now study the structure of such L . As we demonstrated, every eigenpair (λ, v) of L must have matching eigenpair $(1/\lambda, Jv)$. Let $v_1, \dots, v_\kappa, Jv_1, \dots, Jv_\kappa, u_1, \dots, u_{D-2\kappa}$, where $Ju_i = \pm u_i$ are invariant under J . For each eigenvector u_i , $\lambda = 1$ is forced, thus distinct eigenvalues can only come from the 2-cycles. Displaying J in this basis, we have

$$J = \begin{bmatrix} 0 & I & 0 \\ I & 0 & 0 \\ 0 & 0 & D \end{bmatrix}$$

The first $2\kappa \times 2\kappa$ block has signature (κ, κ) , yielding the desired claim. \square

Lemma 24 (Second Order Convergence). *Let $r \in (0, 1)$, $\|R_i\| \leq C\alpha r^i$, X_0, X_1 commute with J . Then, for any $\varepsilon > 0$, there exists $\delta > 0$ such that $X_i \rightarrow L_\alpha$, $\|L_\alpha - I\| < \varepsilon$.*

Proof. That X_i has a limit L_α for α small follows immediately from Lemma 23. Thus it suffices to verify that $\lim_{i \rightarrow \infty} X_i = I$ for the unperturbed sequence. Indeed, if for i large enough, $\|X_i - I\| < \varepsilon$, $\|X_{i-1} - I\| < \varepsilon$, because X_i is polynomial in X_0, X_1, R_j , $j = 1, \dots, i-1$, it follows that it is smooth for α small, thus incurring additional $O(\alpha)$ error. In combination with Lemma 20, this verifies the claim.

Without perturbations, the whole sequence commutes, and

$$J(\eta X_i + (1-\eta)X_{i-1})^{-1}J = (\eta X_i + (1-\eta)X_{i-1})^{-1}J^2 = (\eta X_i + (1-\eta)X_{i-1})^{-1}$$

hence J factors out, and the convergence is a consequence of Lemma 22. \square

B.3.6 Full Rank Hessian

Our main proof strategy is to reduce the Local EGOP iterations to the form of Proposition 2, so that we can guarantee stable first and second order convergence rates by Lemmas 19 and 24. A straightforward change of variables yields the following. Let H have diagonalization $H = U\Lambda U^T$.

Proposition 3 (H Reduction). *Let $J = \text{sign}(\Lambda)$ be the diagonal signature matrix and $W = U|\Lambda|^{1/2}$.*

Define the transformation

$$X_i := W^T \Sigma_i W, \quad \tilde{g} := JW^{-1}g, \\ \tilde{T}(X) := JW^{-1}T(W^{-T}XW^{-1})W^{-T}J, \quad \tilde{R}(X) := JW^{-1}R(W^{-T}XW^{-1})W^{-T}J.$$

Then the recurrence for X_i depends only on J :

$$X_{i+1} = t_{i+1}J \left(\tilde{g}\tilde{g}^T + \beta X_i + (1-\beta)X_{i-1} \right. \\ \left. + \beta[\tilde{g}\tilde{T}(X_i)^T + \tilde{T}(X_i)\tilde{g}^T + \tilde{R}(X_i)] \right. \\ \left. + (1-\beta)[\tilde{g}\tilde{T}(X_{i-1})^T + \tilde{T}(X_{i-1})\tilde{g}^T + \tilde{R}(X_{i-1})] \right)^{-1} J$$

Thus we can reduce our recurrence to that studied in Section B.3.5.

Lemma 25 (Schur Complement). Define $u := g/\|g\|$, $\bar{\pi} := uu^T$, $\bar{Q} := I - \bar{\pi}$, $H_{\bar{Q}} = \bar{Q}H\bar{Q}$. Let

$$\alpha_i := u^T \Sigma_i u, \quad \alpha'_i := u^T H \Sigma_i H u, \quad \eta^2 := \|g\|^2, \quad b_i := \bar{Q} \Sigma_i u, \quad b'_i := \bar{Q} H \Sigma_i H u, \\ C_i := \bar{Q} \Sigma_i \bar{Q}, \quad C'_i := \bar{Q} H \Sigma_i H \bar{Q}, \quad R_{b,i} := \eta \bar{Q} T(\Sigma_i) + \bar{Q} R(\Sigma_i) u, \\ \bar{R}_{\alpha,i} := \beta [2\eta u^T T(\Sigma_i) + u^T R(\Sigma_i) u] + (1-\beta) [2\eta u^T T(\Sigma_{i-1}) + u^T R(\Sigma_{i-1}) u], \\ \bar{b}_i = \beta [b'_i + R_{b,i}] + (1-\beta) [b'_{i-1} + R_{b,i-1}], \quad \bar{R}_{C,i} := \beta \bar{Q} R(\Sigma_i) \bar{Q} + (1-\beta) \bar{Q} R(\Sigma_{i-1}) \bar{Q}, \\ \bar{S}_i := \beta H_{\bar{Q}} C_i H_{\bar{Q}} + (1-\beta) H_{\bar{Q}} C_{i-1} H_{\bar{Q}} + \bar{R}_{C,i} - \frac{1}{\eta^2 + \alpha_i + \bar{R}_{\alpha,i}} \bar{b}_i \bar{b}_i^T.$$

Then, in the orthonormal basis $\{u\} \oplus \text{range}(\bar{Q})$,

$$\begin{bmatrix} \alpha_{i+1} & b_{i+1}^T \\ b_{i+1} & C_{i+1} \end{bmatrix} = t_{i+1} \\ \begin{bmatrix} \frac{1}{\eta^2 + \alpha'_i + \bar{R}_{\alpha,i}} + \left(\frac{1}{\eta^2 + \alpha'_i + \bar{R}_{\alpha,i}} \right)^2 \bar{b}_i^T \bar{S}_i^{-1} \bar{b}_i & -\frac{1}{\eta^2 + \alpha'_i + \bar{R}_{\alpha,i}} \bar{b}_i^T \bar{S}_i^{-1} \\ -\bar{S}_i^{-1} \bar{b}_i \frac{1}{\eta^2 + \alpha'_i + \bar{R}_{\alpha,i}} & \left(\beta C'_i + (1-\beta) C'_{i-1} + \bar{R}_{C,i} - \frac{1}{\eta^2 + \alpha_i + \bar{R}_{\alpha,i}} \bar{b}_i \bar{b}_i^T \right)^{-1} \end{bmatrix}.$$

Proof. This is the Schur complement with pivot on the top-left scalar applied to $M_i := [\beta \mathcal{L}(\mu_i) + (1-\beta) \mathcal{L}(\mu_{i-1})]^{-1}$. \square

Corollary 3 (Base Case). Suppose that $\Sigma_0 = \alpha I$ and $t_1 = \alpha^2$. Then, in the (u, \bar{Q}) basis,

$$\Sigma_1 = \begin{bmatrix} \frac{\alpha^2}{\eta^2} + O(\alpha^3) & O(\alpha^2) \\ O(\alpha^2) & \alpha(\bar{Q}H^2\bar{Q})^{-1} + O(\alpha^2) \end{bmatrix}, \quad \Sigma_2 = \begin{bmatrix} \frac{\alpha^2}{\eta^2} + O(\alpha^3) & O(\alpha^2) \\ O(\alpha^2) & \alpha H_{\bar{Q}}^{-1} H^2 H_{\bar{Q}}^{-1} + O(\alpha^2) \end{bmatrix}$$

Proof. This can be directly computed from the formula in Lemma 25. As a subtle detail, at the first step, the covariance is isotropic, hence in the $\bar{Q} \times \bar{Q}$ block the dominant terms is $\alpha(\bar{Q}H(I)H\bar{Q})^{-1} = \alpha(\bar{Q}H^2\bar{Q})^{-1}$, however, after this step the gradient element of the covariance is a higher order residual, being of the Lemma 19 constant shift form, and thus subsequently $\bar{Q}H\Sigma_1H\bar{Q} = (\bar{Q}H\bar{Q})\Sigma_1(\bar{Q}\Sigma_1\bar{Q}) + O(\alpha^2) =: H_{\bar{Q}}\Sigma_1H_{\bar{Q}} + O(\alpha^2)$. \square

Proof of Theorem 1. We seek to inductively apply Lemmas 19 and 24 to the $u \times u$ and $\bar{Q} \times \bar{Q}$ blocks respectively, necessitating a careful tabulation of the residuals and off-diagonals. Our inductive hypothesis is that

$$\alpha_i = \Theta(t_i), \quad b_i = O(\sqrt{t_i}), \quad C_i = \Theta(\sqrt{t_i}), \quad \bar{R}_{C,i} = O(t_i), \quad \bar{R}_{b,i} = O(\sqrt{t_i}), \quad \bar{R}_{\alpha,i} = O(\sqrt{t_i}).$$

We argue by strong induction, with the base case being covered in Corollary 3. We argue one block at a time. First note that $\bar{b}_i^T \bar{S}_i^{-1} \bar{b}_i = O(\sqrt{t_i})$, hence

$$\frac{1}{\eta^2 + \alpha'_i + \bar{R}_{\alpha,i}} + \left(\frac{1}{\eta^2 + \alpha'_i + \bar{R}_{\alpha,i}} \right)^2 \bar{b}_i^T \bar{S}_i^{-1} \bar{b}_i = \frac{1}{\eta^2} + O(\sqrt{t_i}) \implies \alpha_{i+1} = \frac{t_{i+1}}{\eta^2} + O(t_{i+1}^{3/2}).$$

Thus, taking α sufficiently small, we get a uniform $O(t_i)$ bound by Lemma 19 and Proposition 3.

For the $\bar{Q} \times \bar{Q}$ block,

$$C_{i+1} = t_{i+1} \left(\beta H_{\bar{Q}} C_i H_{\bar{Q}} + (1 - \beta) H_{\bar{Q}} C_{i-1} H_{\bar{Q}} + \left[\bar{Q} H \bar{\pi} (\beta \Sigma_i + (1 - \beta) \Sigma_{i-1}) \bar{\pi} H \bar{Q} + \bar{R}_{C,i} - \frac{1}{\eta^2 + \alpha_i + \bar{R}_{\alpha,i}} \bar{b}_i \bar{b}_i^T \right] \right)^{-1}.$$

As the rescaled residual

$$\left[\bar{Q} H \bar{\pi} (\beta \Sigma_i + (1 - \beta) \Sigma_{i-1}) \bar{\pi} H \bar{Q} + \bar{R}_{C,i} - \frac{1}{\eta^2 + \alpha_i + \bar{R}_{\alpha,i}} \bar{b}_i \bar{b}_i^T \right] / \sqrt{t_i} \leq C \sqrt{t_i} = C \alpha r^i$$

is uniformly summable in α , we can apply Propositions 2 and 3, and Lemma 23 to verify $C_{i+1} = \Theta(\sqrt{t_i})$.

Moving on to the off-diagonal, $-\frac{1}{\eta^2 + \alpha_i + \bar{R}_{\alpha,i}} \bar{b}_i^T \bar{S}_i^{-1} = O(1)$, thus upon multiplying by t_{i+1} , this is $O(t_i)$, whereas the subsequent remainder terms $R_{b,i+1} = \Theta(\|\Sigma_{i+1}\|) = O(\sqrt{t_{i+1}})$. Thus, the contribution is negligible at the following iteration, and the uniform rate follows.

We can immediately plug these rates into our risk bounds to yield $\sqrt{\det \Sigma_i} = \Theta(t_i^{(D+1)/4})$, $W(\mu_t) = O(t_i)$, thus yielding the desired rate. \square

B.3.7 Noisy Manifold

We start off by iterating Corollary 1 as described in the text.

Lemma 26 (Weak Dependence). *Suppose that for all $v \in \text{Null}$, $\eta \in \text{Null}^\perp$, $\eta^T \Sigma v = O(\|\Sigma_{\text{Null}^\perp}\|^2)$. Then, for $\Sigma_{\text{Null}^\perp} := \pi_{\text{Null}^\perp} \Sigma \pi_{\text{Null}^\perp}$, $\Sigma_{\text{Null}} := \pi_{\text{Null}} \Sigma \pi_{\text{Null}}$ there exists $H_{\Sigma_{\text{Null}}}$, $T_{\Sigma_{\text{Null}}}$ such that*

$$\mathcal{L}(\mu) = gg^T + H_{\Sigma_{\text{Null}}} \Sigma_{\text{Null}^\perp} H_{\Sigma_{\text{Null}}} + gT_{\Sigma_{\text{Null}}} (\Sigma_{\text{Null}^\perp})^T + T_{\Sigma_{\text{Null}}} (\Sigma_{\text{Null}^\perp}) g^T + R_{\Sigma_{\text{Null}}} (\Sigma_{\text{Null}^\perp}),$$

$$\|T_{\Sigma_{\text{Null}}} (\Sigma_{\text{Null}^\perp})\| = O(\|\Sigma_{\text{Null}^\perp}\|), \quad \|R_{\Sigma_{\text{Null}}} (\Sigma_{\text{Null}^\perp})\| = O(\|\Sigma_{\text{Null}^\perp}\|^2).$$

Proof. Applying our Gaussian ansatz,

$$\Sigma_v := \text{Cov}_{N(x^*, \Sigma)}(X | \pi_{\text{Null}}[X - x^*] = v) = \Sigma_{\text{Null}^\perp} - [\pi_{\text{Null}^\perp} \Sigma \pi_{\text{Null}}] \Sigma_{\text{Null}}^{-1} [\pi_{\text{Null}} \Sigma \pi_{\text{Null}^\perp}] = \Sigma_{\text{Null}^\perp} + O(\|\Sigma_{\text{Null}^\perp}\|^2).$$

Thus, by Corollary 1,

$$\begin{aligned} \mathcal{L}(\mu_v) &= gg^T + H_v \Sigma_v H_v + gT_v (\Sigma_v)^T + T_v (\Sigma_v) g^T + R_v (\Sigma_v) \\ &= gg^T + H_v \Sigma_{\text{Null}^\perp} H_v + gT_v (\Sigma_{\text{Null}^\perp})^T + T_v (\Sigma_{\text{Null}^\perp}) g^T + R_v (\Sigma_{\text{Null}^\perp}) + O(\|\Sigma_{\text{Null}^\perp}\|^2), \end{aligned}$$

and this latter term can be absorbed into the remainder. Now, integrating out v the relevant operators are

$$H_{\Sigma_{\text{Null}}} = \int H_{\pi_{\text{Null}}[x - x^*]} d\mu(x), \quad T_{\Sigma_{\text{Null}}} = \int T_{\pi_{\text{Null}}[x - x^*]} d\mu(x), \quad R_{\Sigma_{\text{Null}}} = \int R_{\pi_{\text{Null}}[x - x^*]} d\mu(x).$$

\square

While this matrix depends on the Null component of Σ , we will develop a recurrence where this is consistent across iterations. We now expand Lemma 25 in the low-rank Hessian setting.

Lemma 27 (Low-rank Schur). *For $\Sigma = \alpha I$ operators are defined as in Lemma 25, otherwise their equivalents as introduced in Lemma 26. Decomposing in the $(\bar{Q}_{\text{Null}^\perp}, \bar{Q}_{\text{Null}}) := (\text{col}(\bar{Q}) \cap \text{Null}^\perp, \text{col}(\bar{Q}) \cap \text{Null})$ basis, let*

$$\begin{aligned} \tilde{R}_{C,i} &:= \bar{R}_{C,i} - \frac{1}{\eta^2 + \alpha_i + \bar{R}_{\alpha,i}} \bar{b}_i \bar{b}_i^T, \quad \bar{C}_i := \beta C'_i + (1 - \beta) C'_i, \quad A_i = \bar{Q}_{\text{Null}^\perp} \bar{C}_i \bar{Q}_{\text{Null}^\perp} + \bar{Q}_{\text{Null}^\perp} \tilde{R}_{C,i} \bar{Q}_{\text{Null}^\perp}, \\ W_i &= \bar{Q}_{\text{Null}} \tilde{R}_{C,i} \bar{Q}_{\text{Null}} - \bar{Q}_{\text{Null}} \tilde{R}_{C,i} \bar{Q}_{\text{Null}^\perp} [\bar{Q}_{\text{Null}^\perp} \bar{C}_i \bar{Q}_{\text{Null}^\perp}]^{-1} \bar{Q}_{\text{Null}^\perp} \tilde{R}_{C,i} \bar{Q}_{\text{Null}}. \end{aligned}$$

$$C_{i+1} = t_{i+1} \begin{bmatrix} A_i^{-1} + A_i^{-1} [\bar{Q}_{\text{Null}^\perp} \tilde{R}_{C,i} \bar{Q}_{\text{Null}}] W_i^{-1} [\bar{Q}_{\text{Null}} \tilde{R}_{C,i} \bar{Q}_{\text{Null}^\perp}] A_i^{-1} & -A_i^{-1} \bar{Q}_{\text{Null}^\perp} \tilde{R}_{C,i} \bar{Q}_{\text{Null}} W_i^{-1} \\ -W_i^{-1} \bar{Q}_{\text{Null}} \tilde{R}_{C,i} \bar{Q}_{\text{Null}^\perp} A_i^{-1} & W_i^{-1} \end{bmatrix}$$

Proof. Recall that $C_{i+1} := t_{i+1}(\bar{C}_i + \tilde{R}_{C,i})^{-1}$, hence this is the block Schur complement in the specified basis pivoted on the $\bar{Q}_{\text{Null}^\perp} \times \bar{Q}_{\text{Null}^\perp}$ block. \square

Corollary 4 (\bar{Q} block). *Suppose that $\Sigma_0 = \alpha I$ and $t_1 = \alpha^2$. Then, in the $(\bar{Q}_{\text{Null}^\perp}, \bar{Q}_{\text{Null}})$ basis*

$$C_1 = \begin{bmatrix} \alpha(\bar{Q}_{\text{Null}^\perp} H^2 \bar{Q}_{\text{Null}^\perp})^{-1} + O(\alpha^2) & O(\alpha) \\ O(\alpha) & \alpha^2[\bar{Q}_{\text{Null}} \tilde{R}_{C,0} \bar{Q}_{\text{Null}}]^{-1} + O(\alpha) \end{bmatrix},$$

$$C_2 = \begin{bmatrix} \alpha H_{\bar{Q}_{\text{Null}^\perp}}^{-1} H^2 H_{\bar{Q}_{\text{Null}^\perp}}^{-1} + O(\alpha^2) & O(\alpha) \\ O(\alpha) & \alpha^2[\bar{Q}_{\text{Null}} \tilde{R}_{C,1} \bar{Q}_{\text{Null}}]^{-1} + O(\alpha) \end{bmatrix}.$$

The matrix $\alpha^2[\bar{Q}_{\text{Null}} \tilde{R}_{C,i} \bar{Q}_{\text{Null}}]^{-1} = \Theta(1)$, $i = 0, 1$.

Proof. We can once again check this via direct computation utilizing Lemma 27. As \bar{C}_0 comprises terms linear in Σ_0 , it is $\Theta(\alpha)$, meanwhile the remainder terms $\tilde{R}_{C,0} = O(\alpha^2)$. Hence $A_0 = \bar{Q}_{\text{Null}^\perp} \bar{C}_0 \bar{Q}_{\text{Null}^\perp} + O(\alpha^2)$, $W_i = \bar{Q}_{\text{Null}} \tilde{R}_{C,i} \bar{Q}_{\text{Null}} + O(\alpha^3)$, and the remaining approximations directly follow. As in the proof of Lemma 3, at the first step, the covariance is isotropic, hence in the $\bar{Q}_{\text{Null}^\perp} \times \bar{Q}_{\text{Null}^\perp}$ block the dominant terms is $\alpha(\bar{Q}_{\text{Null}^\perp} H(I) H \bar{Q}_{\text{Null}^\perp})^{-1} = \alpha(\bar{Q}_{\text{Null}^\perp} H^2 \bar{Q}_{\text{Null}^\perp})^{-1}$, however, after this step the gradient element of the covariance is a higher order residual, being of the Lemma 19 constant shift form, and thus subsequently $\bar{Q}_{\text{Null}^\perp} H \Sigma_1 H \bar{Q}_{\text{Null}^\perp} = (\bar{Q}_{\text{Null}^\perp} H \bar{Q}_{\text{Null}^\perp}) \Sigma_1 (\bar{Q}_{\text{Null}^\perp} H \bar{Q}_{\text{Null}^\perp}) + O(\alpha^2) =: H_{\bar{Q}_{\text{Null}^\perp}} \Sigma_1 H_{\bar{Q}_{\text{Null}^\perp}} + O(\alpha^2)$. \square

Corollary 5 (Noisy Manifold Base Case). *Suppose that $X_0 = \alpha I$ and $t_1 = \alpha^2$. In the basis $(g, \bar{Q}_{\text{Null}^\perp}, \bar{Q}_{\text{Null}})$, we have*

$$\Sigma_1 = \begin{bmatrix} \frac{\alpha^2}{\eta^2} + O(\alpha^3) & O(\alpha^2) & O(\alpha) \\ O(\alpha^2) & \alpha(\bar{Q}_{\text{Null}^\perp} H^2 \bar{Q}_{\text{Null}^\perp})^{-1} + O(\alpha^2) & O(\alpha) \\ O(\alpha) & O(\alpha) & \Theta(1) \end{bmatrix},$$

$$\Sigma_2 = \begin{bmatrix} \frac{\alpha^2}{\eta^2} + O(\alpha^3) & O(\alpha^2) & O(\alpha) \\ O(\alpha^2) & \alpha H_{\bar{Q}_{\text{Null}^\perp}}^{-1} H^2 H_{\bar{Q}_{\text{Null}^\perp}}^{-1} + O(\alpha^2) & O(\alpha) \\ O(\alpha) & O(\alpha) & \Theta(1) \end{bmatrix}.$$

Proof. Corollary 4 accounts for the bottom right 2×2 block, what remains is to verify the top and left rows. Specifically, we must verify how

$$C_1(b_0 + R_{b,0}) := \alpha^2 \left(\alpha H_{\bar{Q}}^2 + \bar{R}_{C,0} - \frac{1}{\eta^2 + \alpha_0 + \bar{R}_{\alpha,0}} \bar{b}_0 \bar{b}_0^T \right)^{-1} (b_0 + R_{b,0})$$

decomposes across $\bar{Q}_{\text{Null}^\perp}, \bar{Q}_{\text{Null}}$. Applying Corollary 4, we can express this block-wise as

$$\begin{bmatrix} O(\alpha^2) \\ O(\alpha) \end{bmatrix} = \begin{bmatrix} O(\alpha) & O(\alpha) \\ O(\alpha) & O(1) \end{bmatrix} \begin{bmatrix} O(\alpha) \\ O(\alpha) \end{bmatrix}$$

yielding the desired rates. The proof for Σ_2 is essentially the same. \square

Define $\mu(\zeta) = N(x^*, [\Sigma - \Sigma_{\text{Null}^\perp}] + \zeta \bar{Q}_{\text{Null}})$, i.e. the distribution with Null \times Null component fixed to ζ .

Lemma 28 (Filtered Null). *Assume that $D \geq 2d$ and $\text{rank}(H) = 2d$. Let*

$$\Sigma_{i+1} = t_{i+1}[\beta \mathcal{L}(\mu_i(\zeta)) + (1 - \beta) \mathcal{L}(\mu_{i-1}(\zeta))]^{-1}$$

$\sqrt{t_i} = \alpha r^i$, $0 < r < 1$, $\beta > 0$. Then, for α, ζ sufficiently small, $g^T \Sigma_i g = \Theta(t_i)$, for $v \in \text{Null}$, $v^T \Sigma_i v = \Theta(1)$, and for $\eta \in \text{Null}^\perp \cap g^\perp$, $\eta^T \Sigma \eta = \theta(\sqrt{t})$.

Proof. Applying Corollary 1, we can express

$$\mathcal{L}(\mu) = \int \mathcal{L}(\mu_v) d\nu(v) = \int H_v \Sigma_v H_v + g T_v (\Sigma_v)^T + T(\Sigma_v)^T + R_v(\Sigma_v) d\nu(v),$$

where ν is the marginal density $\nu(v) = p_\mu(\pi_{\text{Null}}[X - x^*] = v)$.

We can apply Corollary 5 to verify that the desired anisotropy is present starting from an isotropic initialization. We first study the modified recurrence where the metric M is in terms of $\mathcal{L}'(\mu)$ rather than the EGOP. We proceed by induction to verify that these rates are maintained. Our inductive hypothesis is that

$$\begin{aligned} \alpha_i &= \Theta(t_i), & b_i &= O(\sqrt{t_i}), & C_i &= \Theta(\sqrt{t_i}), & \bar{R}_{C,i} &= O(t_i), \\ \bar{R}_{b,i} &= O(\sqrt{t_i}), & \bar{R}_{\alpha,i} &= O(\sqrt{t_i}), & \|\bar{Q}_{\text{Null}^\perp} \Sigma \bar{Q}_{\text{Null}}\| &= O(\sqrt{t_i}). \end{aligned}$$

The weak Null, Null^\perp corelation allows us to apply Lemma 26 to reduce the recurrence to the marginal form

$$\mathcal{L}(\mu_\zeta) = gg^T + H_\zeta \Sigma_{\text{Null}^\perp} H_\zeta + gT_\zeta(\Sigma_{\text{Null}^\perp})^T + T_\zeta(\Sigma_{\text{Null}^\perp})g^T + R_\zeta(\Sigma_{\text{Null}^\perp}).$$

By assumption $H_0 = H$ is maximal rank, hence for ζ sufficiently small this property is maintained for H_ζ , and we restrict our analysis to this neighborhood. The verification for the $g \times g$ block is exactly the same as verified in Theorem 1 as it is of constant shift form (see Lemma 19), thus we move on to the remaining terms. Explicit computations are similar to those previously presented in Corollaries 4 and 5. First, we immediately have that

$$A_i = H_{\bar{Q}_{\text{Null}^\perp}} [\beta C_i + (1 - \beta)C_{i-1}] H_{\bar{Q}_{\text{Null}^\perp}} + O(t_i), \quad W_i = \bar{Q}_{\text{Null}} \tilde{R}_{C,i} \bar{Q}_{\text{Null}} + O(t_i^{3/2}).$$

Thus for the middle block, applying Lemma 27 yields

$$\bar{Q}_{\text{Null}^\perp} C_{i+1} \bar{Q}_{\text{Null}^\perp} = t_{i+1} \{ H_{\bar{Q}_{\text{Null}^\perp}} [\beta(\bar{Q}_{\text{Null}^\perp} C_i \bar{Q}_{\text{Null}^\perp}) + (1 - \beta)(\bar{Q}_{\text{Null}^\perp} C_{i-1} \bar{Q}_{\text{Null}^\perp})] H_{\bar{Q}_{\text{Null}^\perp}} + O(t_i) \}^{-1}.$$

by the reductions from Propostions 2 and 3, we can reduce this to an autonomous recurrence in $\bar{Q}_{\text{Null}^\perp} C_i \bar{Q}_{\text{Null}^\perp}$ that converges at the desired rate by Lemma 23. See the the proof of Theorem 1 for more details.

Applying Lemma 27 again yields

$$\bar{Q}_{\text{Null}} C_{i+1} \bar{Q}_{\text{Null}} = t_{i+1} W_i^{-1} = t_{i+1} (\bar{Q}_{\text{Null}} \tilde{R}_{C,i} \bar{Q}_{\text{Null}})^{-1} + O(\sqrt{t_i}).$$

As $\bar{Q}_{\text{Null}} \tilde{R}_{C,i} \bar{Q}_{\text{Null}} = O(\|\Sigma_{\text{Null}^\perp}\|^2) = O(t_i)$, it follows that $t_{i+1} (\bar{Q}_{\text{Null}} \tilde{R}_{C,i} \bar{Q}_{\text{Null}})^{-1} = \Omega(1)$, and thus it is of constant order by our covariance cap. Thus this rate is an immediate consequence of the second order anisotropy, and the orthogonal component and other remainders only contribute negligibly, justifying the uniform rate. The remaining terms in the Lemma 27 block decomposition are

$$\bar{Q}_{\text{Null}^\perp} \Sigma_{i+1} \bar{Q}_{\text{Null}} = \bar{Q}_{\text{Null}^\perp} C_{i+1} \bar{Q}_{\text{Null}} = -t_{i+1} A_i^{-1} (\bar{Q}_{\text{Null}^\perp} \tilde{R}_{C,i} \bar{Q}_{\text{Null}}) W_i^{-1}, \quad b_{i+1} = u^T \Sigma_{i+1} \bar{Q} = C_{i+1}(b_i + R_{b,i}),$$

for $u = g/\|g\|$ the normalized gradient vector. In the first term, the product $(\bar{Q}_{\text{Null}^\perp} \tilde{R}_{C,i} \bar{Q}_{\text{Null}}) W_i^{-1} = \Theta(1)$, hence the rate is dominated by the second order anisotropy $t_{i+1} A_i^{-1} = \Theta(\sqrt{t_i})$. For the final vector, $\|b_i + R_{b,i}\| = O(\|\Sigma_{\text{Null}^\perp}\|)$, hence we can combine this with our previous analysis to yield

$$\bar{Q}_{\text{Null}} C_{i+1} (b_i + R_{b,i}) = \Theta(1) O(\sqrt{t_i}) = O(\sqrt{t_{i+1}}), \quad \bar{Q}_{\text{Null}^\perp} C_{i+1} (b_i + R_{b,i}) = \Theta(t_{i+1}) O(\sqrt{t_i}) = O(t_{i+1}).$$

Note that the scalar inflation to go from t_i to t_{i+1} does not aggregate across iterations as the initial bound was driven by the second order anisotropy term, to which the remainders only contribute negligibly. \square

This verifies the claim for the recurrence in $\mathcal{L}(\mu_\zeta)$. Our goal now is to lift this analysis to $\mathcal{L}(\mu)$ with covariance cap ζ . The distinction between these recurrences is that the first a priori filters the Null direction out of the dynamics, whereas the latter trims any eigenvalues above a set threshold ζ . These recurrences coincide if the Null \times Null component never falls below the threshold ζ , thus we seek to identify such a threshold.

Proof of Theorem 3. Lemma 28 verifies the specified dynamics, particularly the Null \times Null component of $\Sigma_{i,\zeta}$ remains $\Theta(1)$, and thus there is some floor $\gamma(\zeta)$ which it never drops below. We now will argue that $\gamma(\zeta) > 0$ as $\zeta \rightarrow 0$, hence there exists a threshold ζ^* such that the filtered and cap dynamics coincide.

As $\zeta \rightarrow 0$, $H_\zeta \rightarrow H$, as the distribution concentrates about x^* , and in particular, for ζ small enough, the signature of H_ζ is the same as that of H . This follows from the maximal rank assumption on H . By Propositions 2 and

3, upon transforming $C_{i,\zeta} \mapsto \frac{W_{\zeta}^T C_{i,\zeta} W_{\zeta}}{\sqrt{c(r,\beta)t_i}} =: X_{i,\zeta}$, $W_{\zeta} := U_{\zeta} |\Lambda_{\zeta}|^{1/2}$, for the diagonalization $H_{\zeta} = U_{\zeta} \Lambda_{\zeta} U_{\zeta}^T$, these recurrences are reduced to the same canonical form, with seeds depending smoothly on ζ . Applying Lemma 21, it follows that $X_{i,\zeta} = X_{i,0} + O(\zeta + \alpha)$.

Inverting the transformation, this yields $C_{i,\zeta} = C_{i,0} + O(\sqrt{t_i}(\delta + \alpha))$. Returning to the proof of Lemma 28,

$$\Sigma_{i,\text{Null},\zeta} = t_{i+1}(\bar{Q}_{\text{Null}} \tilde{R}_{C,i,\zeta}(\Sigma_{i,\text{Null}^{\perp},\zeta}) \bar{Q}_{\text{Null}})^{-1} + O(\sqrt{t_i}) = \Sigma_{i,\text{Null}^{\perp},0} + O(\sqrt{t_i}(\zeta + \alpha)),$$

hence for ζ, α sufficiently small the noise floor is non-vanishing as desired.

Thus the rates of Lemma 28 is achieved. Plugging these rates into our risk bounds yields $\sqrt{\det \Sigma_i} = \Theta(t_i^{(2d+1)/4})$, $W(\mu_t) = O(t_i)$, thus yielding the desired rate. \square

C Extended Discussion

The most obvious problem left open in our approach is the question of accurate EGOP estimation. One path to achieve this is to show that function gradients can also be estimated accurately up to the prescribed error rates in the domains of interest. At initialization, this is of course reasonable, as we focus on a small isotropic region for which the analysis is standard, and an estimator can achieve a fixed level of bias at an $O(n^{-1/2})$ rate. However, in the iteration that immediately follows this can no longer be expected. As a canonical setting, consider the second order anisotropy $g^T \Sigma_i g = \Theta(t_i)$, $v^T \Sigma_i v = \Theta(\sqrt{t_i})$, $v \perp g$. What must be verified is how the elongation impacts pointwise gradient estimates.

When regressing on such an oblique region, the estimated gradient corresponds to the average of the gradients on the ellipsoid. Thus, even if the anisotropy induces bias, it is reasonable to expect that the AGOP, the aggregate of the resulting estimated gradient outerproducts, is very similar to the EGOP. Indeed, we anticipate that the EGOP off-gradient components are on the order of $\Theta(\sqrt{t_i})$, the same magnitude as the anticipated bias correction. The supervised noisy manifold hypothesis does not fundamentally change this calculation, as the additional newly introduced non-decaying components of Σ_i correspond exactly to the directions where the gradient remains constant, and thus present a benign factor in gradient estimation.